METHODS FOR PRODUCING OFF-AXIS RATIO TABLES FROM MINI-MULTILEAF COLLIMATOR SHAPED CIRCULAR FIELDS FOR INPUT INTO A STEREOTACTIC RADIOSURGERY TREATMENT PLANNING SYSTEM

By

BRANDON RICE

A THESIS PRESENTED TO THE GRADUATE SCHOOL
OF THE UNIVERSITY OF FLORIDA IN PARTIAL FULFILLMENT
OF THE REQUIREMENTS FOR THE DEGREE OF
MASTER OF SCIENCE

UNIVERSITY OF FLORIDA

2005

To my loving family and friends, who have believed in and supported me throughout my academic career and life.

ACKNOWLEDGMENTS

I would like to acknowledge my research advisor, Dr. Frank Bova, for his support and insight on this project. I am also much indebted to Drs. David Hintenlang, David Gilland, James Dempsey, and Wesley Bolch for the many hours of insightful lecture and guidance pertaining to medical physics. I would also like to thank the rest of the faculty and staff in the Nuclear and Radiological Engineering Department at the University of Florida, for giving me the opportunity to learn and expand in a collegial environment.

TABLE OF CONTENTS

LIST OF TABLES

LIST OF FIGURES

Abstract of Thesis Presented to the Graduate School
of the University of Florida in Partial Fulfillment of the
Requirements for the Degree of Master of Science

METHODS FOR PRODUCING OFF-AXIS RATIO TABLES FROM MINI-MULTILEAF COLLIMATOR SHAPED CIRCULAR FIELDS FOR INPUT INTO A STEREOTACTIC RADIOSURGERY TREATMENT PLANNING SYSTEM

By

Brandon Rice

August, 2005

Chair: Frank Bova
Major Department: Nuclear and Radiological Engineering

Radiosurgery beam profiles must be determined accurately to avoid complications in critical structures adjacent to the tumor. A micro-multileaf collimator (mMLC) may be used in place of conventional circular collimators to approximate the circular fields typically used in stereotactic radiosurgery. We investigated two methods for producing off-axis ratio tables from the mMLC shaped circular beams for input into the in-house treatment-planning system at the University of Florida.

The first method involves direct measurement of the fields with radiographic film. The second method uses an empirically-based algorithm to model the off-axis ratios. This was accomplished by measuring and characterizing several rectangular fields produced by the mMLC. So-called negative field(s) were calculated and added to a model of a rectangular field to arrive at the final beam model. We were able to accurately model the off-axis ratios for mMLC shaped circular beams to within (0.5 mm) distance-to-

agreement error in high gradient regions and (3%) dose-dose error elsewhere in the beam profile for at least 90% of the points in each field. Given its simplicity and accuracy, we believe this method for modeling off-axis ratios of radiosurgical beam profiles is ideal.

CHAPTER 1
BACKGROUND

Overview of Stereotactic Radiosurgery

Stereotactic radiosurgery (SRS) is a single dose fraction form of radiotherapy that relies on the ability to accurately deliver a high dose of radiation to a stereotactically identified target.[1] It is an accepted modality for treating a variety of neurologic conditions such as benign, primary, and metastatic tumors and arteriovenous malformations.[2] Although distinctly different from fractionated radiotherapy or routine neurosurgery, SRS can be considered a hybrid of both.

Conventional radiotherapy seeks to eliminate diseased tissue by delivering small doses of radiation in many fractions (normally 1 or 2 fractions per day), through several static radiation fields.[2-3] Fractionated treatments increase damage to the tumor because of reoxygenation and reassortment of cells into more sensitive phases of the cell cycle. Inaccurate beam and patient positioning is inherent in common radiotherapy planning and must be considered when developing a treatment plan. Subclinical, or microscopic disease processes that do not show up on diagnostic images must also be accounted for. Consequently, a large amount of healthy tissue is typically encompassed in the treatment plan to account for positioning errors and microscopic disease.[2] This can lead to a large amount of healthy tissue being irradiated at the target dose and possibly destroyed, leading to patient complications years down the road. For example, if a 2 cm diameter brain lesion is planned with a 5 mm margin of error to account for positioning errors, an

additional 7 cm^3 of healthy tissue is encompassed in the treatment plan; this additional healthy tissue represents approximately 70% of the total target volume.

Stereotactic radiosurgery works to avoid these pitfalls of conventional radiation therapy by administering a large dose of radiation in one fraction so that the dose distribution has a steep gradient (decreases rapidly spatially) and is conformal to the disease being treated, typically with submillimeter precision (less than 0.5 mm). Radiosurgery relies on accurate, stereotactically targeted delivery and steep dose gradients; it does not rely on taking advantage of radiobiological differences between normal and diseased tissue.[2]

Stereotactic radiosurgery also differs from common neurosurgery. Neurosurgery is an invasive, in-patient process that seeks to physically remove the pathological process. The neurosurgeon almost immediately knows whether or not a complication will occur. Radiosurgery, on the other hand, is a non-invasive, out-patient process. The radiosurgeon does not instantaneously know if there will be delayed complications.[2]

The idea of SRS was conceived in the late 1940s by a Swedish neurosurgeon named Lars Leksell.[1] His concept was to have many small, focused beams of radiation impinge on a single target localized in space. He first achieved this with orthovoltage x-rays and particle beams. He then invented a machine that uses many small sources of radioactive cobalt-60 focused on a single point in space, to provide a large dose of radiation to diseased tissue, while causing little or no harm to healthy tissue only millimeters away. This method of SRS is still performed today using a commercially available system called the Gamma Knife. Our study focused on another technique that uses x-rays from a common linear accelerator (linac) to deliver the dose of radiation.

The steep dose gradient of linac radiosurgery is typically achieved by using a basic concept of geometric optimization: many small beams are applied semi-isotropically about a target and are directed to converge on the target. A large dose will be delivered where the beams overlap and will fall off rapidly outside of this area.

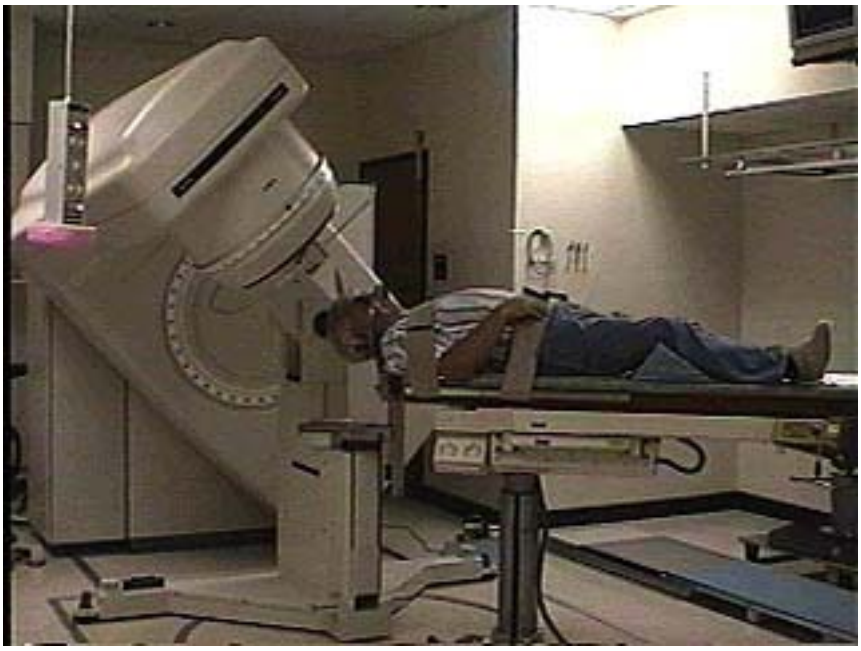

Figure 1-1. Linac SRS. The linac delivers a high dose of radiation with a series of precisely placed arcs to control the lesion while sparing healthy tissue.

A rigid frame of reference is needed to relate the center of the imaged target to the linac isocenter. The isocenter is the point of intersection of rotation of the gantry, patient couch, and collimator. Three-dimensional computed tomography (CT) image reconstructions are used to stereotactically identify the target within the patient anatomy. This is often used in conjunction with other imaging modalities, such as angiography (a 2-D imaging modality) and magnetic resonance imaging, to allow for better interpretation of the patient anatomy.

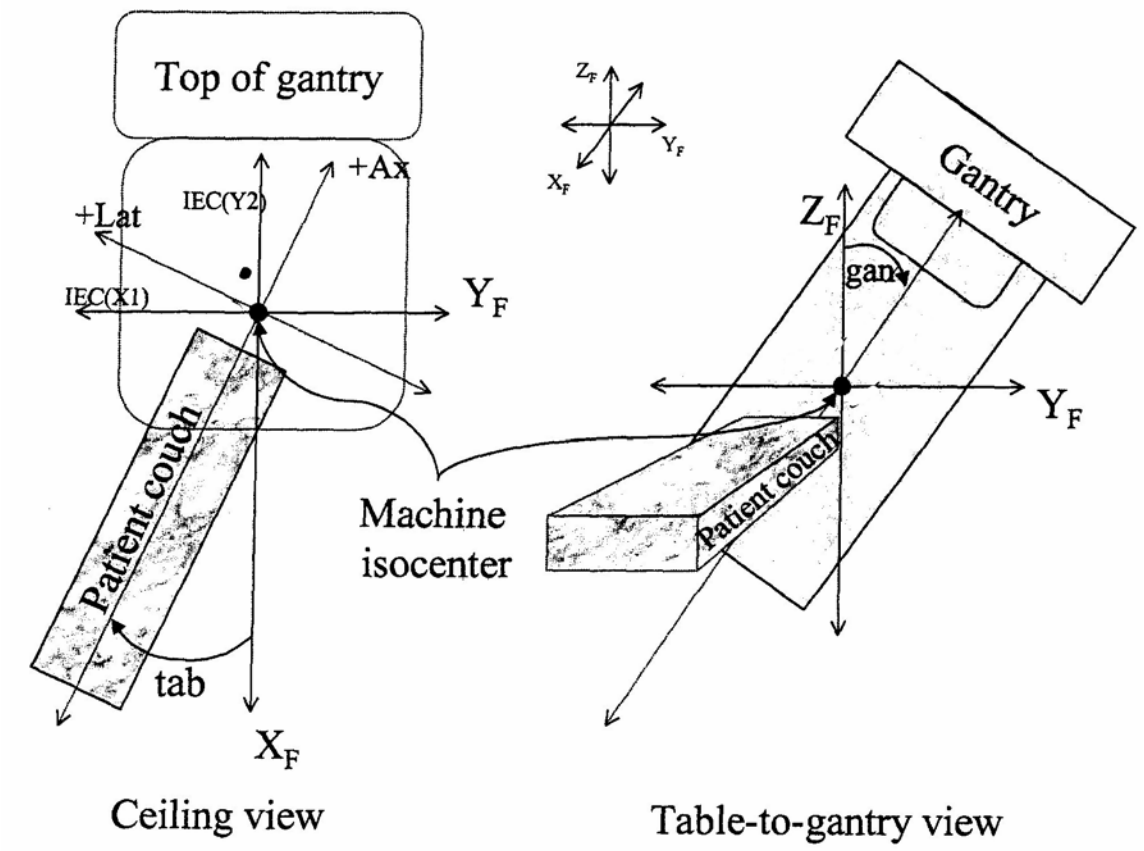

Figure 1-2. Linac isocenter. The isocenter is the point of intersection of the patient couch, gantry, and collimator.

The stereotactic frame is the rigid frame of reference that can be attached to the patient couch or pedestal of the linear accelerator and to the patient's skull.[1] The Brown-Robert-Wells (BRW) frame is a commonly used stereotactic head frame[2] that is used by the radiosurgery team at the University of Florida. The frame has three orthogonal axes that intersect at the center of the circular frame.[2] The BRW CT frame is equipped with a localizer that has nine fiducial rods which appear as dots in each axial slice of the CT image.[1] The location of these fiducial rods is precisely known; therefore it is possible to relate any point in the CT reconstruction to the reference frame coordinates. Knowing precisely where the target is located with respect to a frame of reference is critical to accomplishing the goals of radiosurgery.

Figure 1-3. BRW head ring and CT localizer mounted on a Styrofoam head.

Delivery Techniques

Several methods are commonly used to shape the small radiation fields and to produce the treatment plans needed to deliver the conformal, high dose of radiation to the target. They include the multiple isocenter technique, micro-multileaf collimator (mMLC) conformal beams, and intensity modulated radiation therapy (IMRT). This section provides a brief background on the multiple isocenter technique; this technique is the most preferred and commonly used delivery method and is the method currently used by the University of Florida SRS team.

The single or multiple isocenter technique for treatment delivery uses one or more sets of noncoplanar arcs of radiation shaped by small, circular collimators, usually less than 3 cm in diameter. This method is ideal for producing nearly spherical or elliptical dose distributions in high-isodose regions (70-80%).[2,4-5] The next discussion expands on delivery techniques used by the University of Florida radiosurgery team.

The width of the dose distribution (size of the radiation field) is approximately the diameter of the circular collimator projected to isocenter. A typical single-isocenter

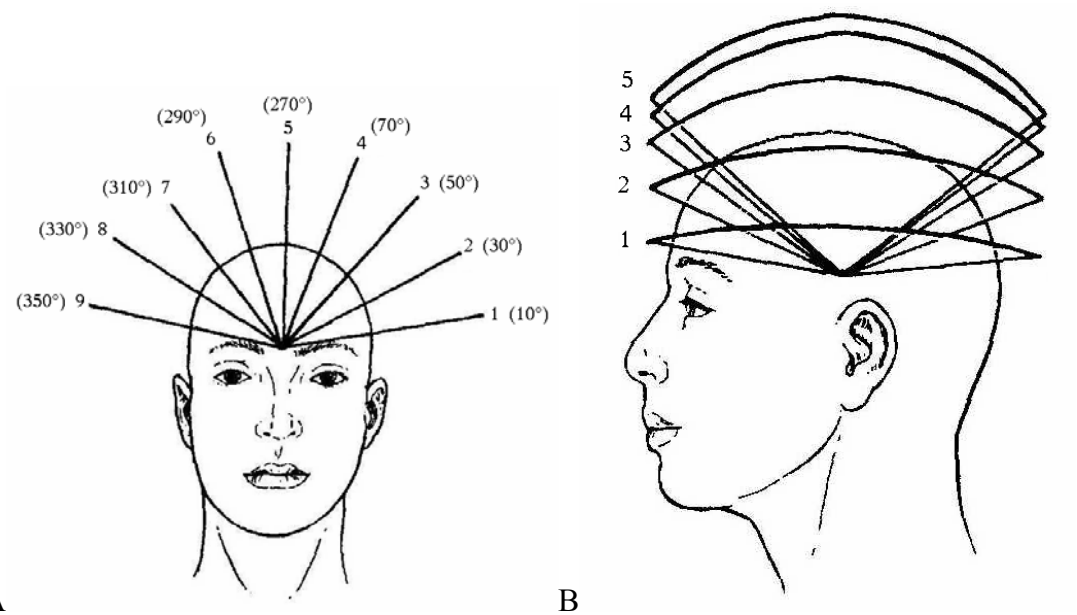

A B

Figure 1-4. A typical single isocenter plan begins with nine equally spaced arcs of radiation. (A-B) Coronal and lateral views of a nine arc set. Angles in (A) refer to patient table angles.

plan consists of 5-9 equally spaced arcs of radiation; each arc span is 100° and the arcs are spaced 20° apart.[2,5] These arcs of radiation are directed to overlap in the target region (at isocenter), taking advantage of the basic concept of geometric optimization discussed earlier. An isocenter in this context refers to a spherically shaped region used to approximate target dimensions and should not be confused with the mechanical isocenter

of a linac. The typical characteristic beam starting angle begins 30° vertical off the superior, and extends 100° to end at 50° vertical off inferior.[2]

In most clinical circumstances, the target or lesion will have an elongated, ellipsoidal, or irregular geometrical shape rather than be perfectly spherical. Sometimes the target will lie adjacent to a critical structure in the brain such as the optic chiasm. To account for these irregularities in target shape and to avoid critical structures in the brain, several parameters can be adjusted to adjust the shape and/or orientation of the dose distribution. Individual beam start and stop angles and arc weights can be adjusted to elongate or shift the orientation of the dose distribution.[2,5] Adjusting these parameters does not drastically alter the shape of the dose distribution. For large or irregular target shapes, more than one isocenter is used to approximate the target. If multiple isocenters are used on a single target, the number of arcs is reduced from 9 to 5 for each isocenter. This is done to save time and produces nearly the same gradient as a nine arc set.[2,5] Using multiple isocenters results in substantial dose inhomogeneity in the high isodose regions.[4,6]

An efficient radiosurgery team such as the one at the University of Florida will spend approximately fifteen minutes treating a single isocenter using this technique, even though the actual beam on time for this treatment lasts a few minutes. A collision test must be performed after each table rotation to ensure the linac does not collide with the patient upon gantry rotation. A major drawback to this technique is the large amount of time it takes to treat multiple isocenters. Many cases involve more than one isocenter; on average the treatment time is one hour, but treatment time can take up to several hours for the most complicated cases with many isocenters.

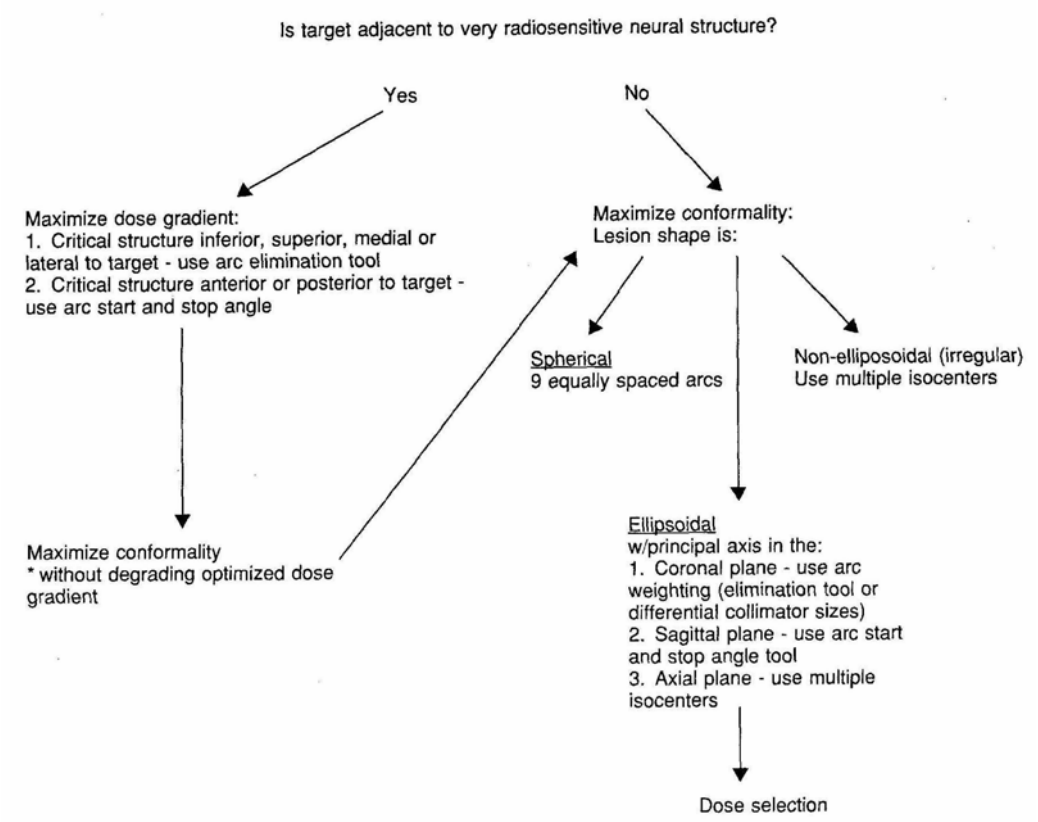

Figure 1-5. The University of Florida SRS treatment planning algorithm.

Multileaf collimators (MLCs) may be used to approximate the circular fields produced by circular collimators.[7] Multileaf collimators have been used to shape radiation fields for many years. They consist of two arrays of tungsten leaves; each leaf is driven individually by its own motor. Recently, multileaf collimators have been developed with SRS in mind. The main factor separating conventional MLCs and MLCs specifically designed for radiosurgery is leaf width. Multileaf collimators designed for radiosurgery have leaf widths typically on the order of a few millimeters, whereas the leaf width on conventional MLCs is over a centimeter. Hence, MLCs designed for radiosurgery are usually referred to as mini or micro-multileaf collimators (mMLC).

St. John investigated how the finite leaf width of the mMLC affects the conformality and gradient of dose distributions. He showed that mMLC leaf width can

have a considerable effect on the ability to use a mMLC to approximate circular beams.[7] For example, a 5 mm circle cannot be approximated accurately using an MLC with 1 cm wide leaves. The leaves on the mMLC used in our study are approximately 5 mm wide projected to isocenter. It has been shown that dose distributions produced by mMLCs with 5 mm wide leaves are virtually indistinguishable from those produced by mMLCs with 1 mm leaf widths.[7]

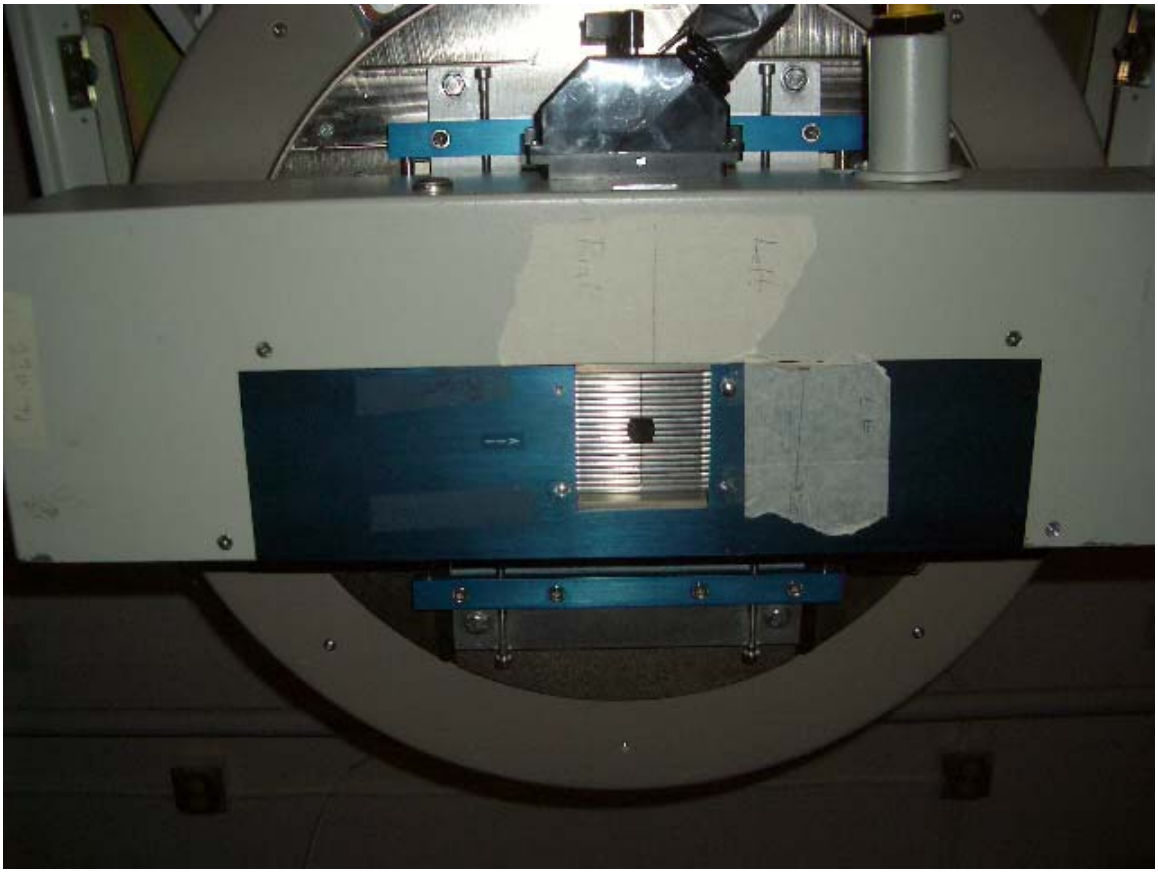

Figure 1-6. Mini-multileaf collimator used in our study. The collimator consists of twenty pairs of tungsten leaves, each driven by an individual motor and controlled by a computer.

Circular fields shaped by a mMLC can be approximated using either an odd or an even set of leaves. The alternative that provides the optimal approximation is governed by the size of the circle being approximated and mMLC leaf width. In the ideal

situation, the mMLC would be allowed to rotate in between arcs to allow for better approximation of the circle. Since this is not the case, the center of the circle being approximated is forced onto a leaf edge or leaf center, whichever is closer. If the center of the circle is on a leaf edge, an even number of leaves will approximate the circle best. If the center of the circle is on a leaf center, an odd set of leaves will work best to approximate the circle (when no collimator rotation is used).

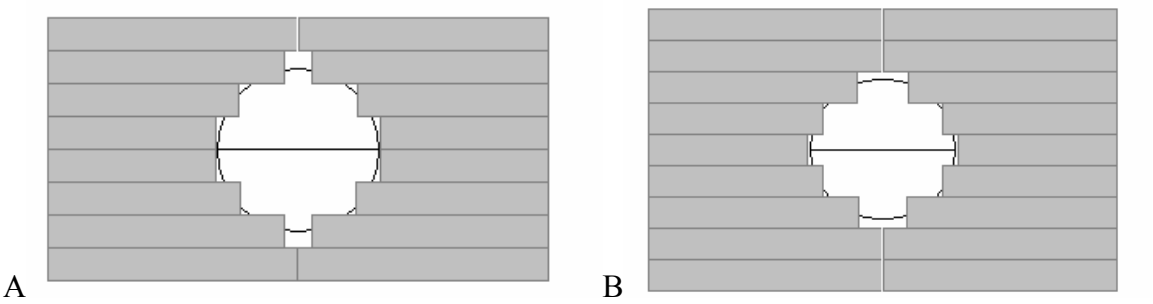

Figure 1-7. Using a micro-multileaf collimator to approximate circles. A) The circle is centered on a leaf edge so an even set of leaves are used. B) The circle is centered on a leaf center so an odd number of leaves are used.

If a mMLC is used to shape the radiation beam, in place of conventional circular collimators, it is possible to drastically reduce the amount of time it takes to treat multiple isocenter targets. This in turn leads to a more optimal and efficient treatment delivery and increased patient satisfaction. For example, consider a treatment plan containing three isocenters (Table 1-1). Using the standard technique with circular collimators, it takes approximately 50 min for the University of Florida radiosurgery team to complete the treatment. Before each separate isocenter is treated, the center of the isocenter (target) is placed at the isocenter of the linac, and the appropriate circular collimator is mounted onto the linac. Also, a collision test must be performed for each table angle.

If a mMLC is used to deliver the treatment, the geometric center of the target is placed at the linac isocenter. This eliminates the need to place the center of each

individual isocenter at the isocenter of the linac. It also eliminates the need to switch out collimators for different isocenters. The mMLC will approximate the shape of the necessary circle for the isocenter being treated. Also, using a mMLC allows all three isocenters to be treated from each table angle, so the collision test needs to be performed a total of five times, as opposed to fifteen times when using the conventional circular collimators.

Table 1-1. Hypothetical treatment plan with three isocenters

	Center Coordinates[a]							
Isocenter Num	AP (mm)	Lat (mm)	Ax (mm)	Arc num	Collim. size (mm)	Table angle	Start angle	End angle
1	-19.0	-15.0	-40.0	1	12	20	30	130
				2	12	55	30	120
				3	12	340	230	330
				4	12	305	240	330
				5	12	270	240	330
2	-21.3	-12.0	-36.0	6	18	20	30	130
				7	18	55	30	120
				8	18	340	230	330
				9	18	305	240	330
				10	18	270	240	330
3	-16.0	-17.5	-43.7	11	10	20	30	130
				12	10	55	30	120
				13	10	340	230	330
				14	10	305	240	330
				15	10	270	240	330

[a]For the conventional technique that uses circular collimators, the center coordinates of each isocenter are placed at the linac isocenter.

Assuming 5 min of initial patient set up, an average of 300 monitor units (MUs) per arc of radiation, and a dose rate of 400 MUs per min, it would take approximately 16 min to complete the treatment with the mMLC; this corresponds to a 70% reduction in the amount of time necessary to complete the treatment. The reduced treatment time becomes more drastic as more isocenters are introduced. A complicated eight isocenter

plan could take over 2 h to treat using standard circular collimators; the plan would take about 40 min to treat using a mMLC.

It has been suggested conformal and IMRT techniques are superior to the multiple isocenter technique for treating complex targets.[6,8-11] The fact is multiple isocenter treatment planning can be difficult and the resulting dose distributions highly user dependent. Inhomogeneous dose distributions and poor target conformality are the result of improperly optimized multiple isocenter plans. Wagner investigated the three methods of radiosurgery treatment delivery by implementing optimization algorithms for each; this way each technique could be compared fairly.[5] The multiple isocenter technique was optimized with a sphere packing algorithm that determined the placement of variably-sized spheres within the target volume.[5] The result of his work showed the multiple isocenter technique was able to produce a highly conformal dose distribution while maintaining a steep dose gradient outside the target volume.[5] For general and complex cases, it was determined that the optimized multiple isocenter technique outperformed the other methods.

Dosimetry

The absorbed dose to a small mass of material is defined as the amount of energy absorbed from charged particles liberated by ionizing radiation per unit mass of material. The kinetic energy released in the medium (KERMA) is defined as the sum of the initial kinetic energies of all the charged ionizing particles liberated by uncharged particles in a material per unit mass.[1] Since charged particles travel a certain distance before depositing their energy, the absorbed dose will increase with depth in the material up to a point where the number of charged particles entering a small volume equals the number of charged particles leaving that volume. This condition is known as charged particle

equilibrium. The absorbed dose then begins to decrease with depth at the same rate of the collision KERMA.

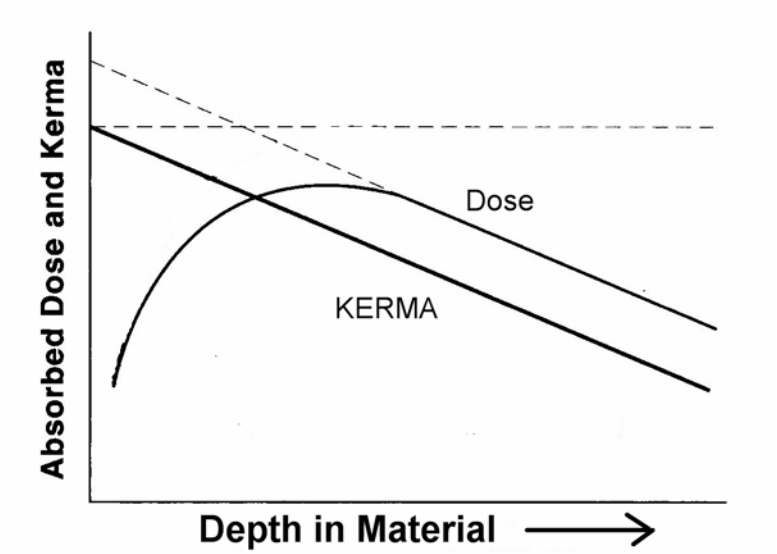

Figure 1-8. Relationship between absorbed dose and collision kerma for a megavoltage photon beam.

For many of the small fields used in radiosurgery, electronic equilibrium does not exist in the lateral direction. This is due to the fact that the size of many of these small fields is smaller than the range of electrons being produced. The resulting loss of electronic equilibrium will occur at every point in the field, even in the center.[12] There are several consequences that must be taken into consideration when dealing with these small fields: the cross-beam profile is flat over only a small fraction of the full width at half maximum, the output factor decreases dramatically with a decrease in field size, and the inverse square law may not hold for large source to point distances.[12] In general, a large percentage of the beam is made up of penumbra.

The SRS treatment planning system at the University of Florida requires the input of several beam parameters. These include output factors, dose rate at isocenter, tissue phantom ratios (TPR) at several depths, and off-axis ratios (OARs) for various sized

fields. These parameters are derived from empirical measurements and data. An accurate assessment of these parameters is essential for minimizing the dose to normal tissues and reducing the risk of complications due to nonconformal dose distributions.

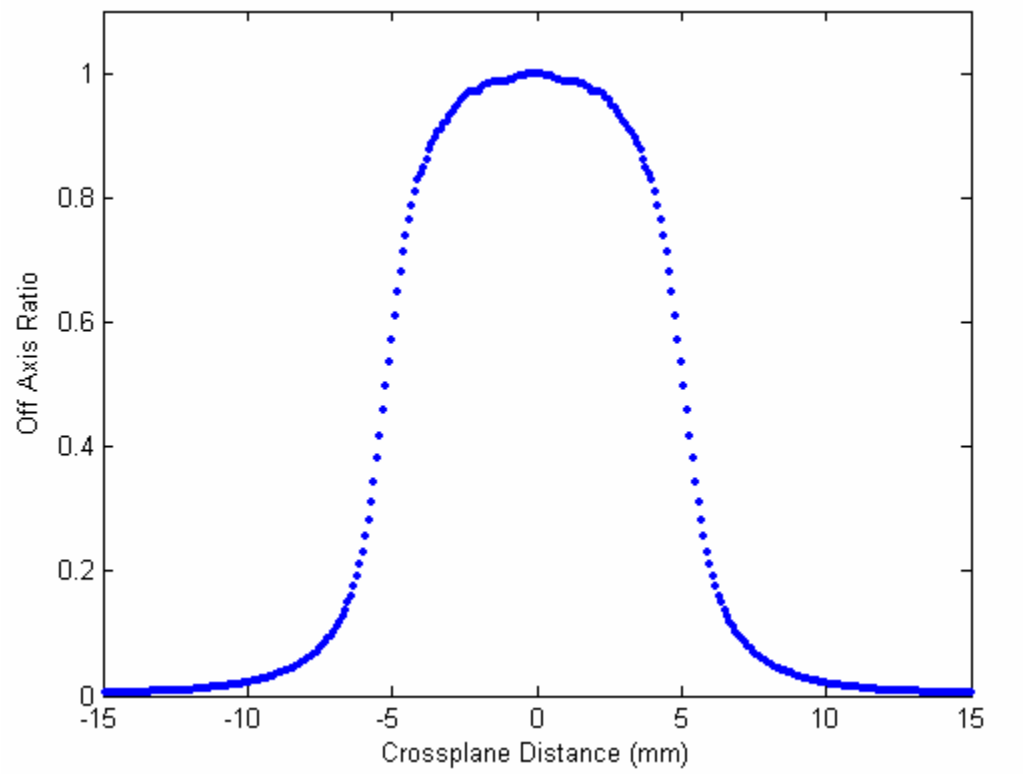

Figure 1-9. Cross-plane off-axis ratio profile for a 12 mm field. Approximately 30% of the field is composed of penumbra.

For any beam centered on the linac's primary axis at the machine isocenter, the absorbed dose to any point is calculated by Equation 1-1.

$$Dose(p) = RD * MU * TPR * OAR * ROF * \left[\frac{ScD}{STD}\right]^2, \qquad (1\text{-}1)$$

where the reference dose (RD) is the dose per monitor unit, MU is the number of moniter units delivered, TPR is the tissue-phantom ratio, OAR is the off-axis ratio, ROF is the relative output factor, ScD is the source to calibration point distance, and STD is the source to target distance.

Our study focused on measuring and modeling off-axis ratios of mMLC shaped circular fields. The empirically driven radiosurgery treatment planning system at the University of Florida requires the input of a two dimensional matrix for each odd or even mMLC shaped field; these matrices have normalized values (between zero and one) and contain the necessary off-axis information for each beam. The previous scheme that used circular collimators required the input of one-dimensional arrays of off-axis ratios. There was no need for a 2-D matrix because the circular fields were perfectly symmetric.

The penumbra of a radiation field refers to the region at the edge (of the field) over which the dose changes rapidly.[1] The penumbra consists of two components: transmission penumbra and geometric penumbra. The transmission penumbra is the region in space exposed to photons that have traveled through part of the collimator. The geometric penumbra is the region that is irradiated by a spatially finite source.[13] The variation in dose at the edge of the field also depends on the amount of scattered radiation within the material of interest. The physical penumbra is thus defined as the spatial distance between two specified points of relative dose, namely 80% and 20% of the dose to the central axis.[13]

The type of detector used to measure the small the fields in radiosurgery should be considered carefully. Lack of electronic equilibrium in the field will cause large detectors to yield erroneous results.[13] The model detector for radiosurgery dosimetry should have several unique qualities. The ideal dosimeter should have submillimeter spatial resolution.[12, 14-16] It should have a dose response that is energy, field size, and dose rate independent.[14] It should provide a spatial map of the dose distribution rather than the dose at a single point, particularly for cases where it is necessary to verify

conformal distributions.[15] Also, the detector should be linear, reproducible, and stable.[14] There is no ideal dosimeter for radiosurgery, but there are several that approach the ideal.

Radiographic film has been used extensively in radiosurgery dosimetry. It is a high resolution dosimeter that records information in two dimensions. Some possible problems that are encountered with film are variations in sensitivity and dose response which results from variable processing conditions.[14] This problem may arise when trying to compare the doses from two separate films; the problem can be overcome by developing films from the same film batch under identical processing conditions.

Radiographic film also suffers from spatial non-uniformity.[14] Spatial variations on the order of 2% are typically seen with radiographic film. A flat area of the measured field may be averaged to reduce the error due to these variations. This correction is not possible when taking penumbra measurements, because the field is changing rapidly over this distance. A final problem encountered with radiographic film is its over-response to low energy photons due to the high atomic number components that make up the film.[12,14] The problem becomes worse as the field size and depth of measurement are increased, resulting in systematic error of the measured dose in the tail of the penumbra.[12] This should not be a significant problem for the small fields typically used in radiosurgery.

Radiochromic film is another type of film that can be used for radiation therapy dosimetry; this type of film does not require chemical developing so it avoids variations in sensitivity and dose response that result from variations in processing conditions.[14] Radiochromic film suffers from disadvantages such as poor reproducibility[14] and long developing time. It takes approximately 24 h for the typical radiochromic film to

develop, so it is not as convenient as conventional radiographic film. Another disadvantage of using radiochromic film is the fact that it does not respond well to low doses of radiation. Radiochromic film also needs to be handled carefully and protected from exposure to sunlight and fluorescent lighting.

Radiographic film does not perfectly fit all the criteria for an ideal dosimeter for SRS, but it comes close. It outperforms common dosimeters such as diodes, ionization chambers, and thermoluminescent dosimeters (TLDs) because film has high spatial resolution and the ability to make a simultaneous measurement of a spatial map of dose. To accurately measure the penumbra of small fields, the detector needs to be small compared to spatial variations in dose. Volume averaging can become a significant problem in even the smallest available ionization chambers.[16] The low cost and general performance characteristics of radiographic film make it a suitable detector for performing relative dosimetric measurements on the small fields used in radiosurgery.

CHAPTER 2
OFF-AXIS RATIO MEASUREMENT OF MINI-MLC APPROXIMATED CIRCLES

Introduction

One possible method of producing the off-axis ratio lookup tables to be used in the radiosurgery dosimetry system is to directly measure them. Although this method can be time consuming, the results are valuable in that they can be used to provide a means for comparison with model calculations. This chapter will go through the methodology used to measure the circular fields formed by mini-multileaf collimators and convert the measurement to a useful off-axis ratio table.

Materials and Methods

A Varian CLINAC 600C 6MV Radiotherapy Accelerator was used to produce the radiations fields that were measured. A miniature multileaf collimator (Wellhofer Dosimetrie, Schwarzenbruck, Germany) was used to shape the radiation fields. The mMLC has 20 pairs of tungsten leaves that project 4.95 mm wide at the isocenter of the linac. Each leaf is stepping-motor driven along a curved path so that ends of the leaves match the beam divergence.[17]

Table 2-1. Physical characteristics of the Wellhofer mini-MLC

Number of leaves	20
Leaf width at isocenter	4.95 mm
Leaf height	8.0 cm
Maximum field size at isocenter	9 X 10 cm^2
Source-to-collimator distance (mounted on the Varian 600C)	65.0 cm
Leaf travel over central axis	2.0 cm
Leaf velocity	1 cm/s
Mass	35 kg

Kodak X-OMAT V radiographic film was used to measure the radiation fields. Each piece of film was placed at the isocenter of the linac on top of a four centimeter slab of solid water which was used to provide sufficient backscatter. A one and a half centimeter slab of solid water was placed on top of the film to provide buildup. The film was located at the depth of maximum absorbed dose. The film was developed in a Kodak M35A-M X-OMAT processor; the temperature of the processing chemicals during film development was always 32.8±0.5°C. Films from measurements performed on the same day were taken from the same film batch and were developed under identical processor conditions to avoid film variations in dose response and sensitivity.

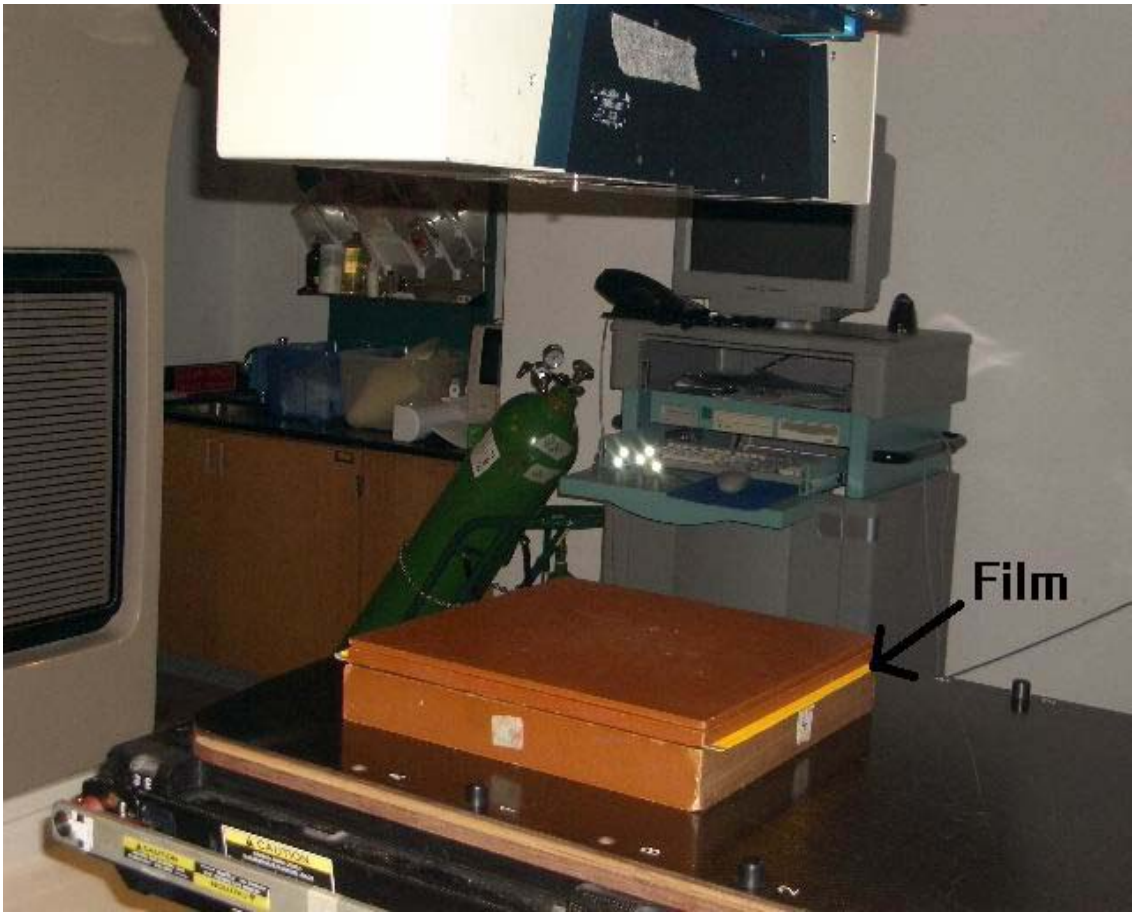

Figure 2-1. Basic setup for film measurements. Kodak radiographic film is sandwiched between two slabs of solid water.

A calibration exposure was produced before a set of film measurements was made to provide a means to convert optical density to dose. The calibration exposure was developed along with the other films; a new calibration exposure was made each day new measurements were taken. The calibration exposures typically contained five or six exposures in the range of ten to eighty monitor units (MUs). The mMLC was set to produce six centimeter square fields for the calibration exposures.

After the calibration film was exposed, the mMLC was set to create circular field approximations using an even number of open leaves; the circular fields produced had diameters ranging from 10 cm to 30 cm in 2 cm increments. Six exposures of each circular approximation were made on the same sheet of film. The calibration film and measurement films were developed in the Kodak processor and scanned with an Epson Expression 1600 flatbed scanner at 0.1 mm/pixel resolution. The films were scanned at a high resolution to preserve the inherent high spatial resolution of the detector.

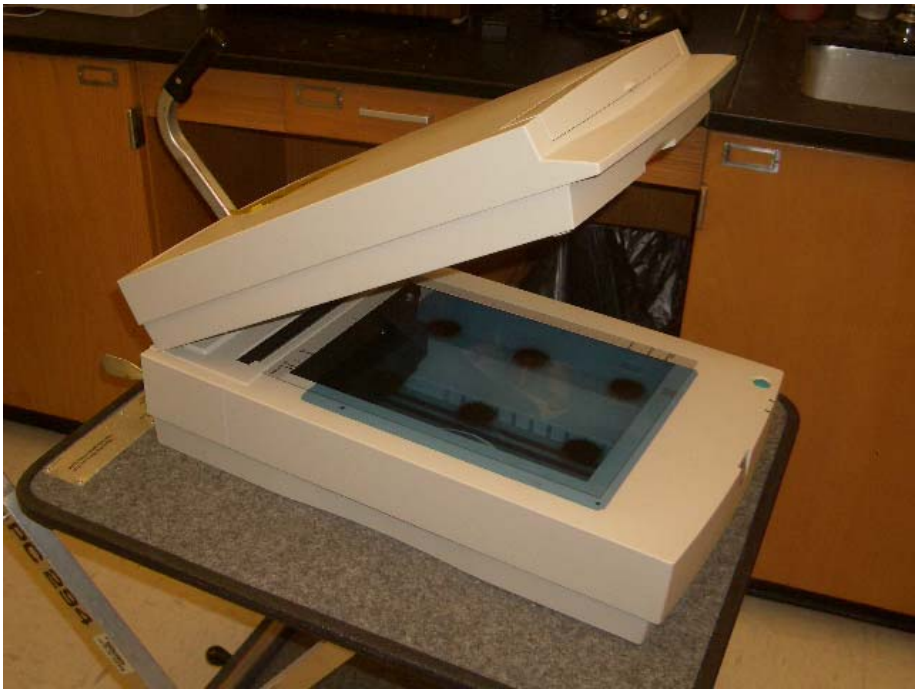

Figure 2-2. Epson flatbed scanner and processed radiographic film.

Several films were scanned on a Lumisys L575 densitometer at 0.124 mm/pixel resolution; this was done to determine if the flatbed scanner would produce the same results as the laser densitometer. It was determined that the flatbed scanner produced similar results to the laser densitometer.

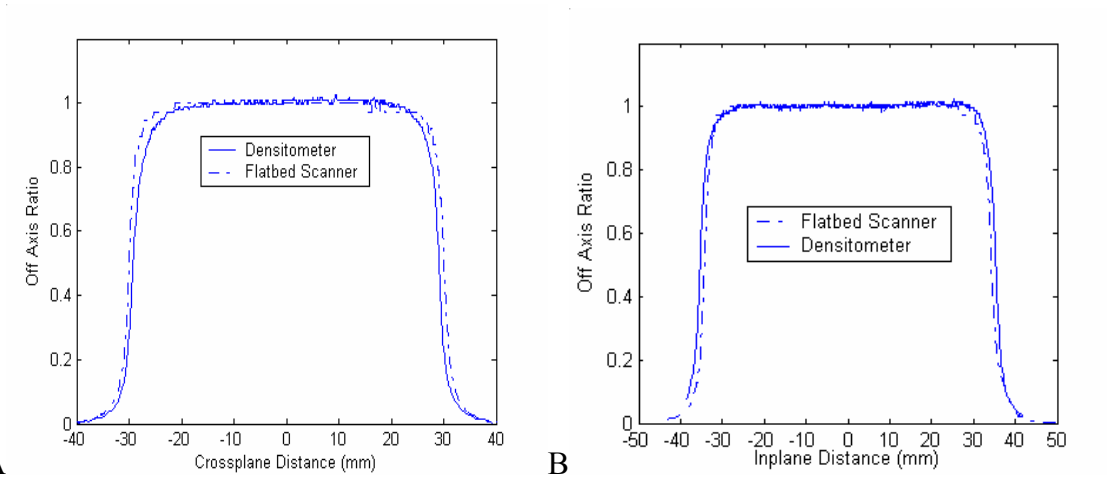

A B

Figure 2-3. Off-axis profile film measurements of a 6 cm by 7 cm rectangular field. The profiles are used to compare the flatbed scanner with the densitometer. A) is a cross-plane (direction of leaf travel) profile and B) is an in-plane (direction of leaf width) profile.

Consistency and uniformity checks were also performed on films scanned by the Epson scanner. A consistency test was performed to determine if the scanning resolution was consistent throughout the length of the scanner. A ruler was scanned at 0.1 mm/pixel resolution and the results were analyzed with a tool developed in Matlab. The tool prompts the user to click on each centimeter marker on the image of the ruler; the program then determines the distance between each marker. The results of the consistency check showed the scanner was performing acceptably, with an average error less than 0.1 mm, which is the size of each pixel. A uniformity check was performed on unexposed radiographic film; the standard deviation of absolute dose was determined to be less than 2%.

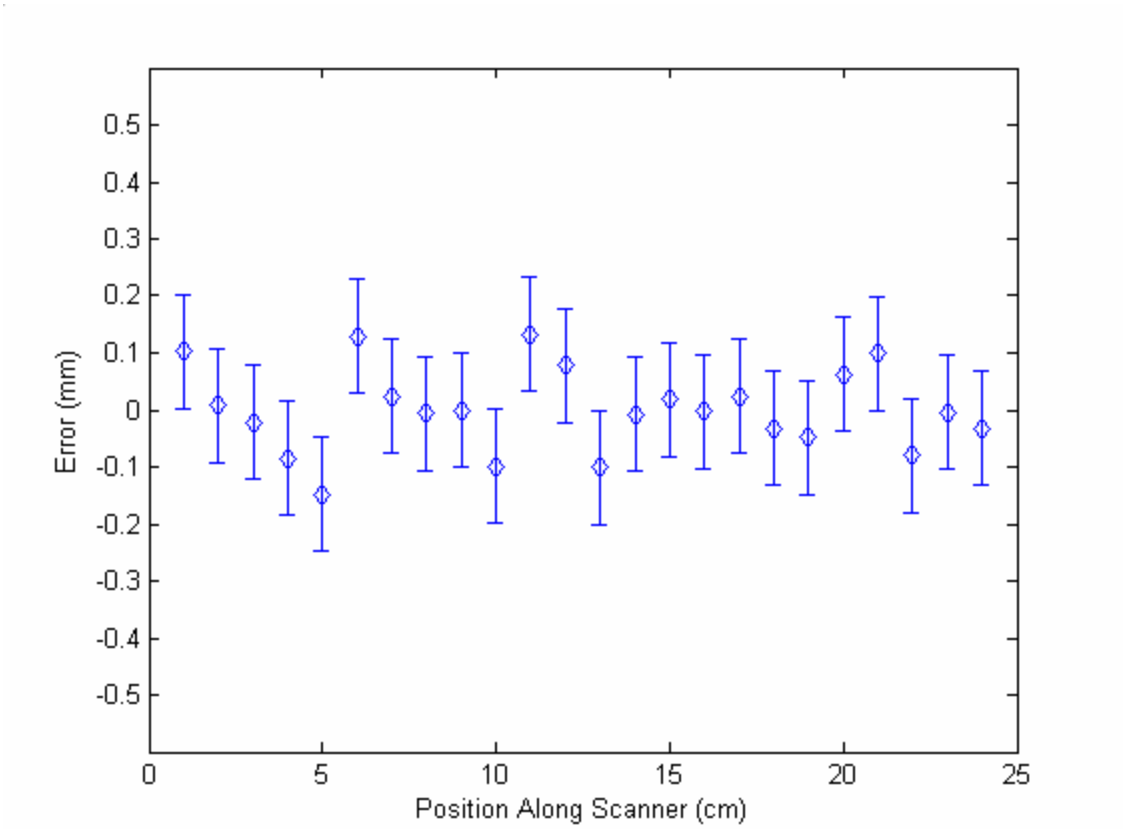

Figure 2-4. Results of the consistency check performed on the Epson flatbed scanner. The average absolute value of position error along the scanned ruler is 0.06 mm.

Once all the films were scanned and saved on the computer, a calibration curve was created to convert optical density to dose. Output factors for rectangular fields produced by the mMLC were measured beforehand with an Exradin 14P ion chamber (parallel plate, 0.002 cm^3 active volume,1 mm window thickness and 1 mm window-collector gap); the output factor for a 6 cm square field was needed to convert monitor units to dose. The linac is calibrated to have a 10 cm square field deliver 1 cGy of radiation dose to water at d_{max} (1.5 cm) per monitor unit. The product of output factor and monitor units yields the amount of dose delivered to the film. The output factor for a 6 cm square field produced by the mMLC was determined to be 0.96; this value is in good agreement with the output of a 6 cm square field (0.957) when the mMLC is not attached.

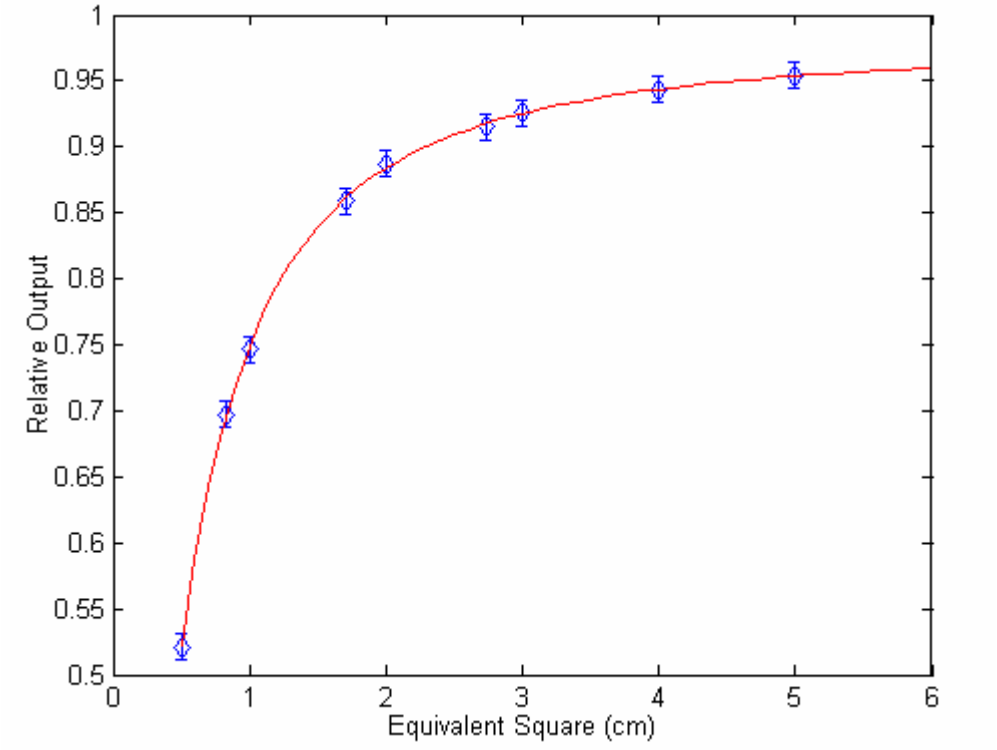

Figure 2-5. Output of rectangular fields shaped by a miniMLC. The output of the field produced by the mMLC is relative to the output of a 10 cm square field produced by the primary collimator jaws alone.

A film calibration tool developed in Matlab by St. John was modified to read in exposures saved in tagged image format (tiff) and to convert pixel value to optical density. Equation 2-1 was used to relate pixel value to optical density for an 8-bit image.

$$\mathbf{OD} = -\log_{10}\left(\frac{\mathbf{P}}{\mathbf{255}}\right), \qquad (2\text{-}1)$$

where OD is optical density and P is the pixel value (between 0 and 255 for an 8-bit grayscale image). The program prompts the user to input the output factor, number of calibration exposures and corresponding monitor units delivered for each exposure. The user is prompted to select each exposure file and click on the background and exposure peaks in an optical density histogram. The average background is determined and

subtracted from each exposure. A second degree polynomial is fit to a plot of dose versus optical density.

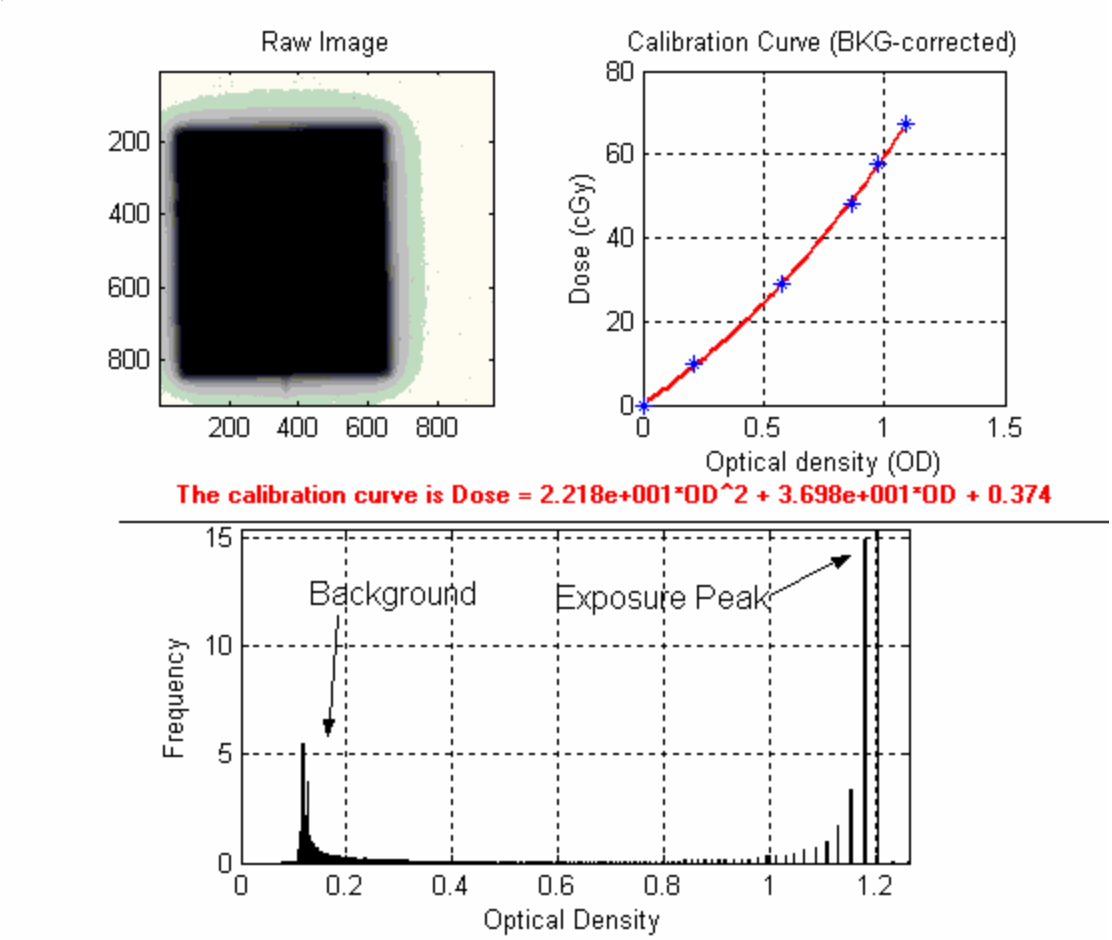

Figure 2-6. Film calibration tool. The user is prompted to click on the background and exposure peaks for each separate exposure.

Another program was developed in Matlab to allow the user to separate, center, and align multiple exposures on a single film. The user inputs the resolution the film was scanned at and number of exposures on the film. After clicking on the (Get Image) button, the user is prompted to select the image file. The program displays the scanned image of the film and prompts the user to box in each exposure with the mouse. After an exposure has been selected, the program displays only the selected image. The user then zooms in on the top, right, bottom, and left sides of the image, respectively. Once a side

is zoomed in on, the user is prompted to click on the center of the edge of the field. Having these four points, the program calculates the equations for the lines of the central axis and the point where the two lines intersect (the center of the beam). The image is then rotated slightly so the central axis of the beam is perpendicular to the sides of the image. Since the center of the beam is known, the program is able to crop the image so the center of the beam is exactly in the center of the image.

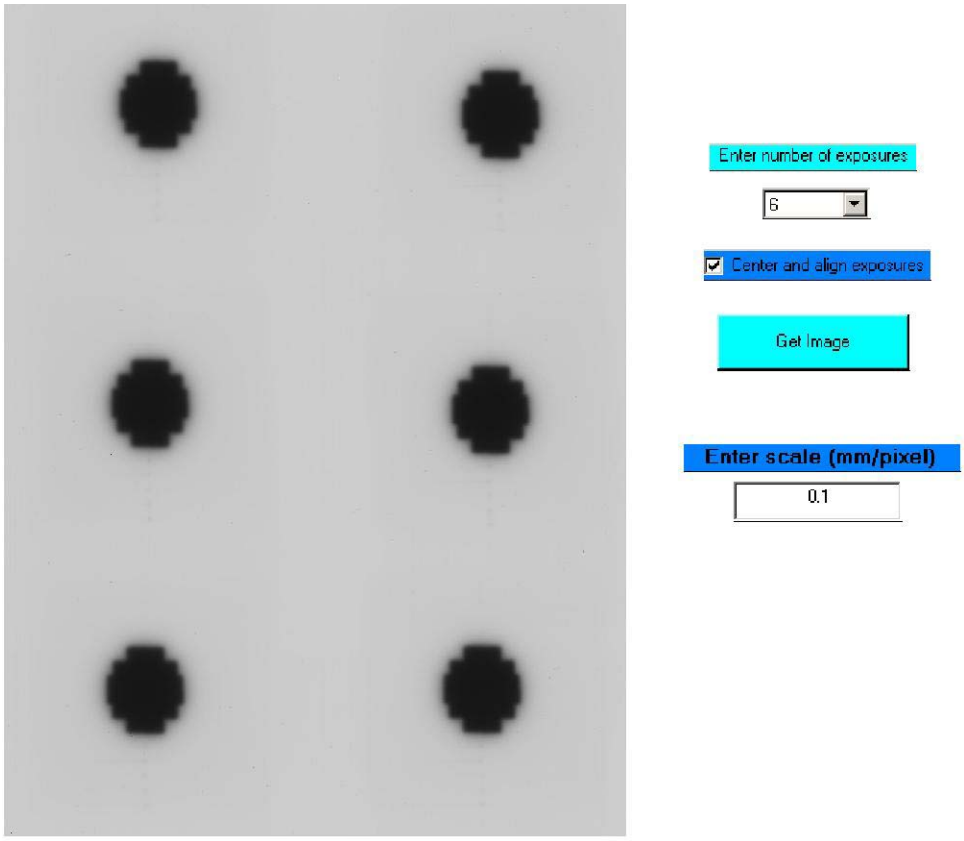

Figure 2-7. Tool used to separate and align exposures. The scanned image contains six 26 mm mMLC circular approximations.

A program was developed to convert optical density to dose and to normalize the dose on a scale between zero and one. Since each quadrant of the mMLC circular field is symmetric about the central axis, the program is able to split up each intensity matrix into four separate but equal quadrants. Since six exposures were made for each field, a total

of 24 field quadrants were produced for each circular field. These quadrants were averaged together by the Matlab program to produce the final result, a two dimensional map of off-axis ratios. Since multiple exposures were averaged together to produce the 2-D maps, it was possible to calculate a 2-D map of statistical uncertainty for each field. The actual error between the measured fields and the real dose distribution is probably less than predicted by statistical uncertainties. This is due to the fact that a spatial error in one quadrant will be somewhat compensated by the resulting opposite spatial error in the adjacent quadrant.

Results

Some typical two dimensional maps of measured off-axis ratios are shown along with their statistical uncertainties in Figures 8-12. The statistical uncertainty has no units (off-axis ratios are unitless) and is generally less than 10% in high gradient (penumbra) regions and less than 2% in low gradient regions. A large uncertainty in the penumbra region is expected due to the rapid falloff of dose. The plots display one quarter of the field with the origin located at the central axis of the field.

Discussion

Circular approximations of radiation fields form by a mMLC were measured with radiographic film; the processed films were input into several Matlab programs designed to separate and center the exposures, convert optical density to dose, and to average field quadrants to arrive at the final result. It was determined the process of separating and aligning exposures introduces the most error to the final result. Some measured off-axis ratio tables had much lower uncertainty than others. This is because the off-axis ratio tables with the lower uncertainty came from exposures that were better aligned.

Exposures may be over or under-rotated by as much as a few degrees. Proper alignment and centering of the exposures is crucial to arriving at an accurate result. A new, less user-dependent, method of aligning the exposures is currently being developed. The new method uses an edge-detection algorithm to find the top, bottom, left, and right edges of the field. Once these edges are determined, the exposures can be rotated accurately, with errors less than 1°.

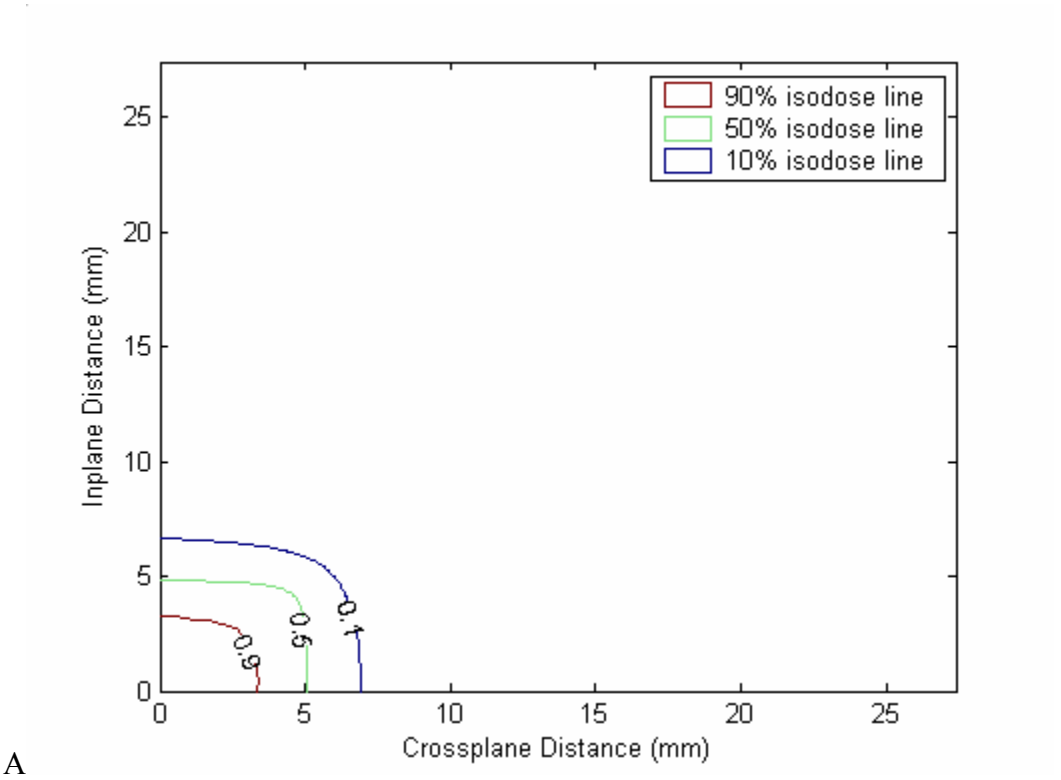

A

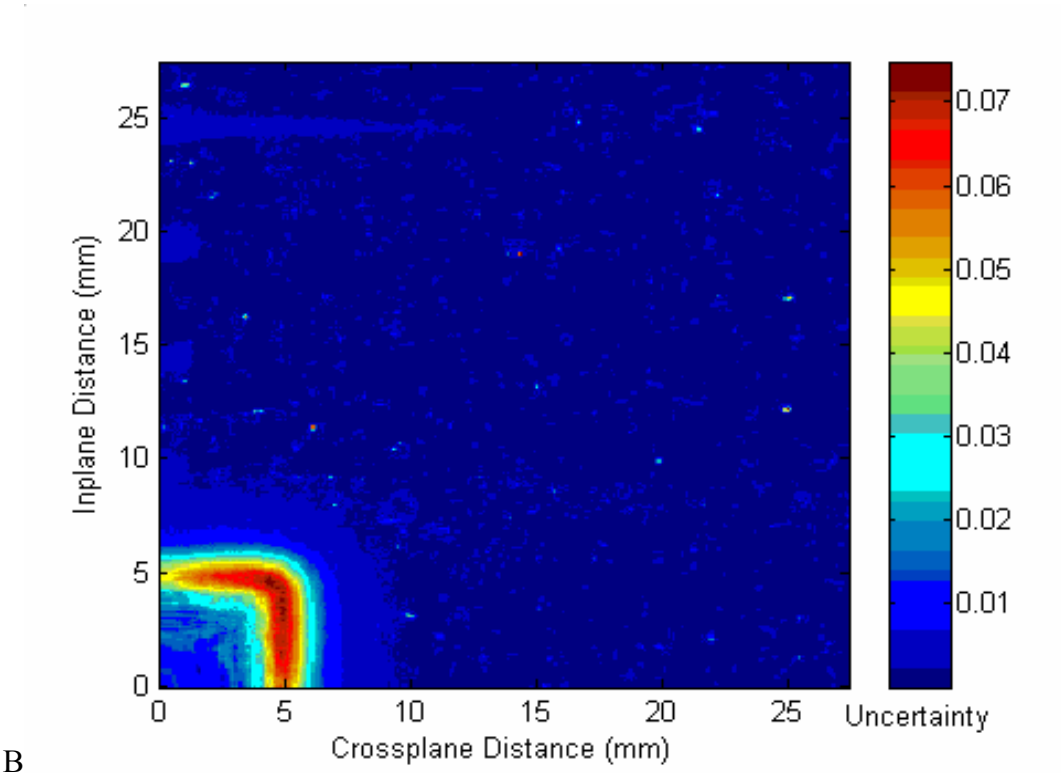

B

Figure 2-8. Twelve millimeter mMLC circular approximation with even leaves. A) is a contour plot of the average measurements and B) is a map of the statistical uncertainty for each pixel in the measurement.

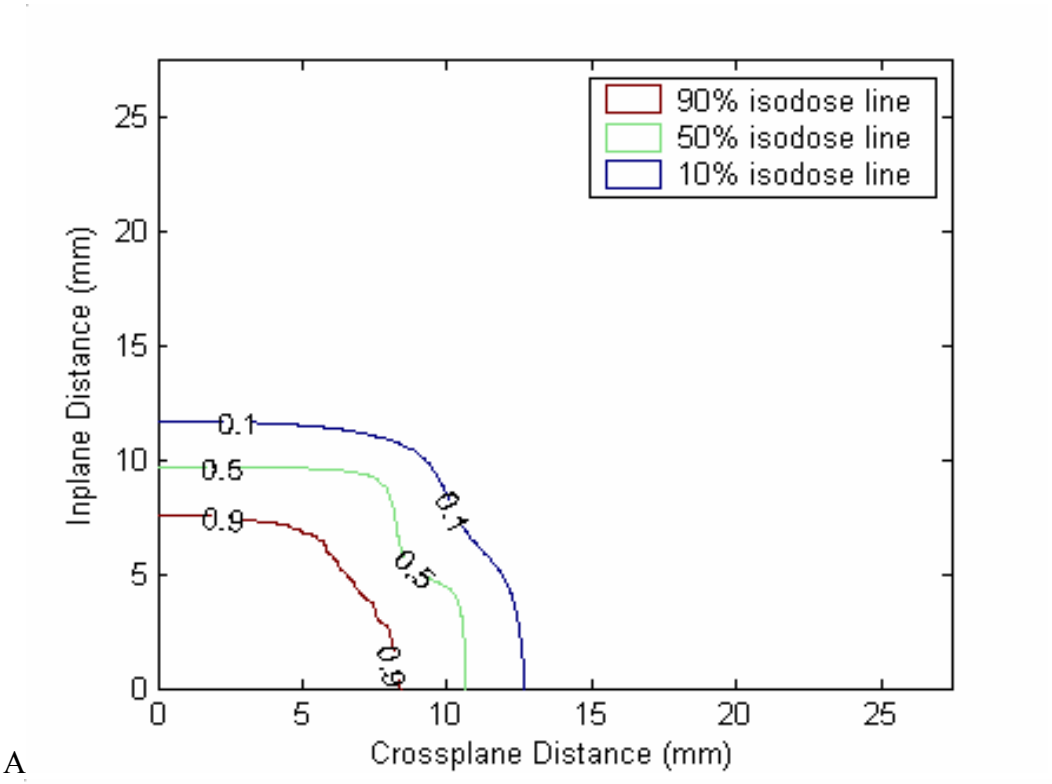

A

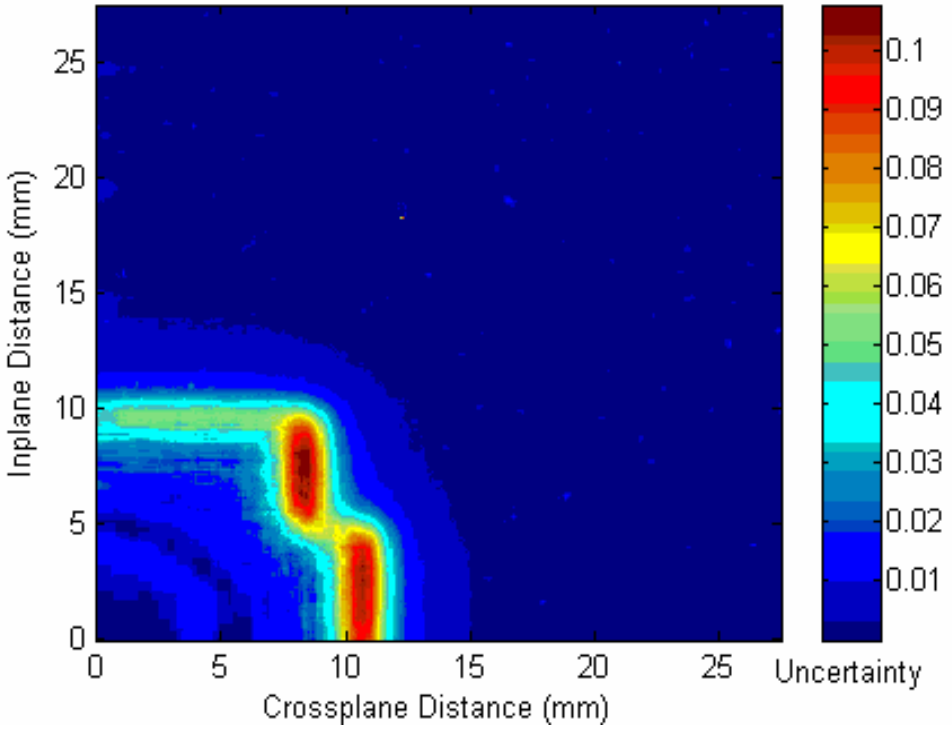

B

Figure 2-9. Twenty two millimeter mMLC circular approximation with even leaves. A) is a contour plot of the average measurements and B) is a map of the statistical uncertainty for each pixel in the measurement.

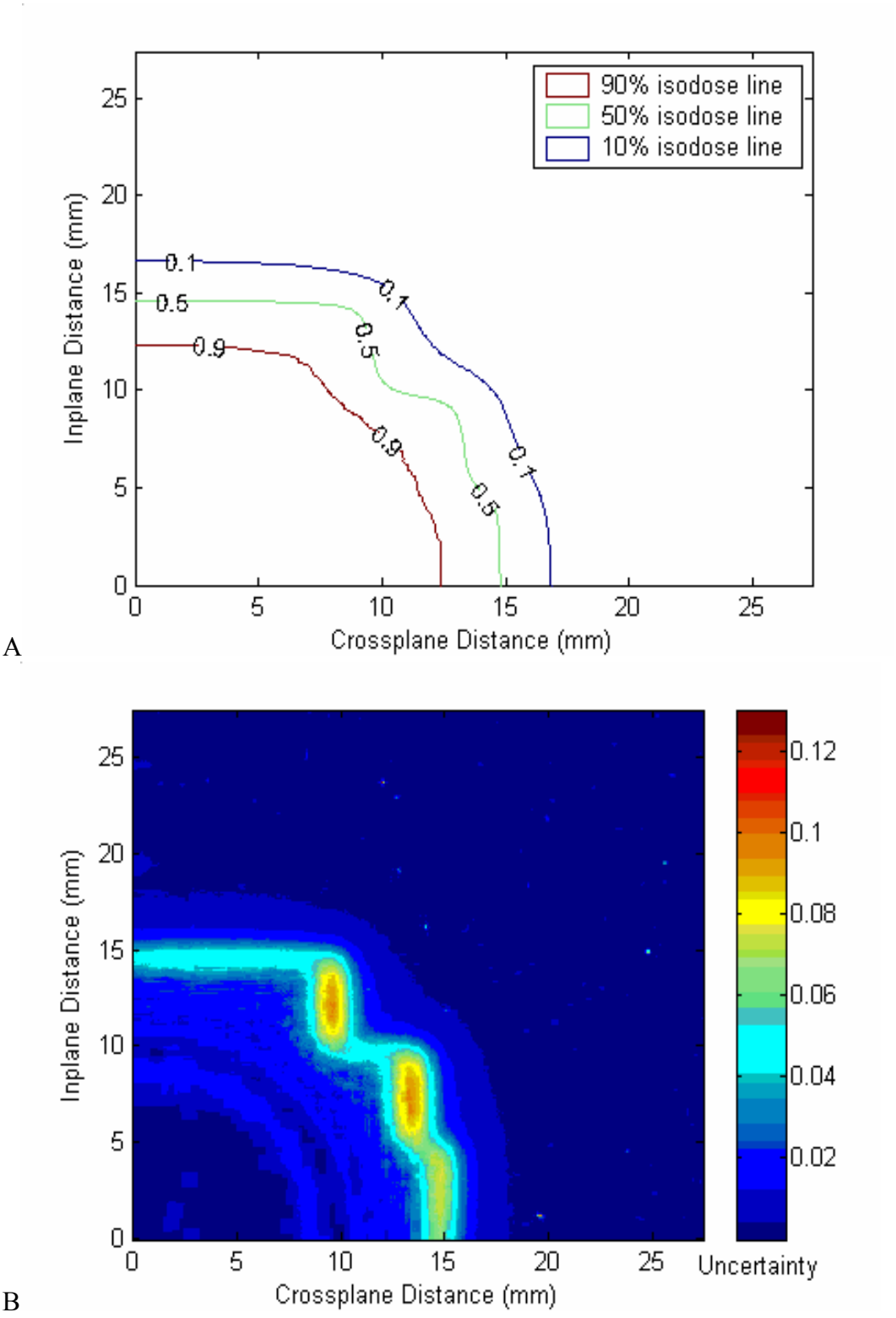

A

B

Figure 2-10. Thirty millimeter mMLC circular approximation with even leaves. A) is a contour plot of the average measurements and B) is a map of the statistical uncertainty for each pixel in the measurement.

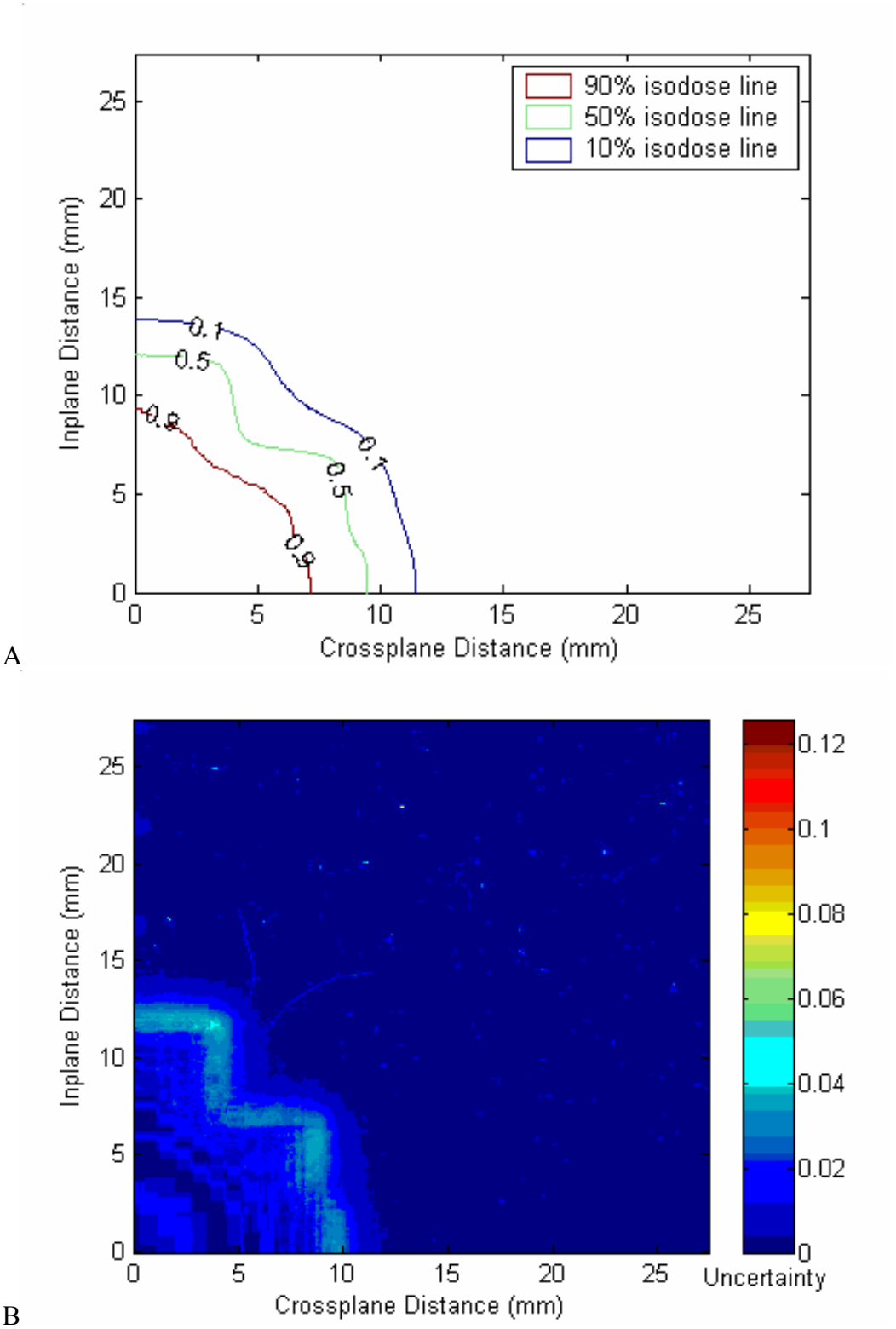

Figure 2-11. Twenty millimeter mMLC circular approximation with odd leaves. A) is a contour plot of the average measurements and B) is a map of the statistical uncertainty for each pixel in the measurement.

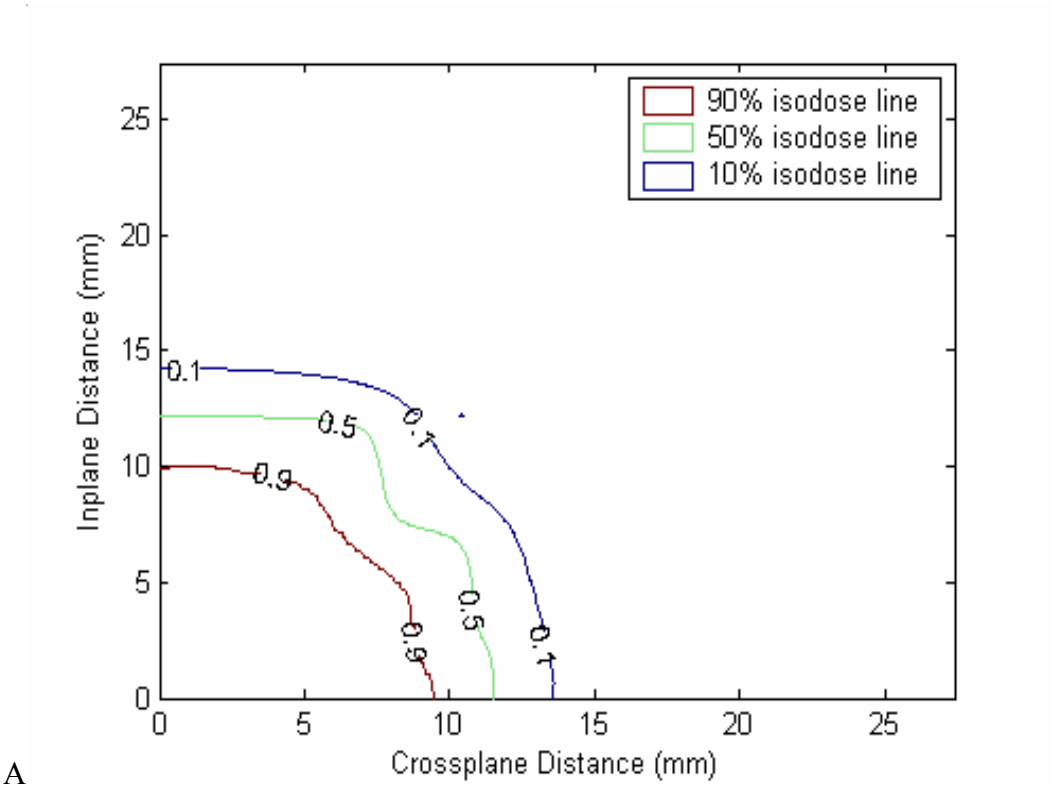

A

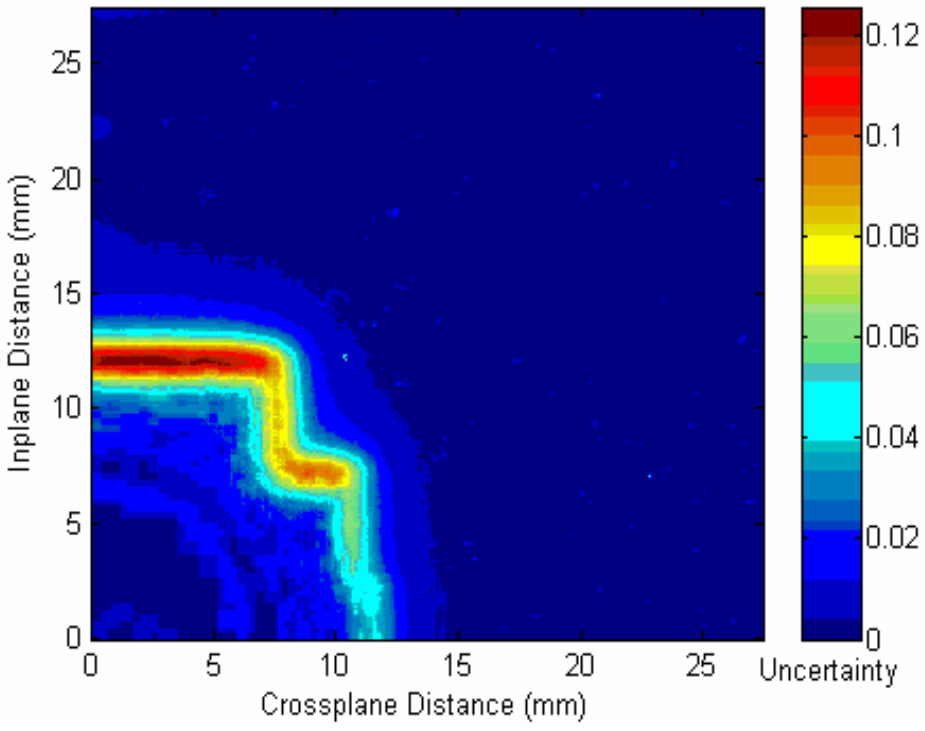

B

Figure 2-12. Twenty four millimeter mMLC circular approximation with odd leaves. A) is a contour plot of the average measurements and B) is a map of the statistical uncertainty for each pixel in the measurement.

CHAPTER 3
A ROBUST ALGORITHM TO MODEL OFF-AXIS RATIOS OF MINI-MLC APPROXIMATED CIRCULAR FIELDS

Introduction

Our goal was to develop a tool to model the off-axis ratios of mMLC shaped circular fields since the direct measurement of these fields is time consuming. The model is then used to produce two-dimensional lookup tables for input into the radiosurgery treatment planning system. One alternative method that could be used to produce the off-axis ratio tables is Monte Carlo simulation, but it would take more time to run Monte Carlo simulations than to perform direct measurements. Also, the validation of Monte Carlo requires the determination of the parameters and then validation of results. Since Monte Carlo does not provide results in a timely manner, another method was considered. This chapter discusses a simple technique that employs model constructions to produce the off-axis ratio tables.

Methods and Materials

The model construction is based on the negative field technique using the basic Cunningham model.[18] This technique involves the application of negative fluences to a rectangular open field to produce the desired dose distribution. The algorithm that was developed to help us achieve our final result is as follows:

- Measure the off-axis ratios of rectangular fields with widths varying over the range of interest (10-30 mm).
- Fit the Cunningham model to the measured off-axis ratios and acquire the necessary fitting parameters.

- Create a model of a rectangular field using the fitting parameters acquired in Step 2.
- Calculate the negative field and subtract the negative field from the rectangular model.
- Repeat Step 4 if there is more than one negative field.

Rectangular fields formed by the mMLC were measured with Kodak X-OMAT V film; the width of the measured rectangular fields varied from 10 mm to 30 mm. Optical density was converted to dose and normalized using the results from a film calibration curve obtained by the film calibration tool. One dimensional cross-plane (in the direction of leaf motion) and in-plane (in the direction of leaf width) profiles through the central axis were determined from the data set. The Cunningham model was fit to cross-plane and in-plane profiles using the curve fit tool in Matlab. The fitting algorithm employs a nonlinear least-squares technique. The Cunningham model for off-axis ratio (OAR) at a point r mm from the central axis is

$$\begin{aligned} \mathbf{OAR} &= \mathbf{1 - 0.5 * \exp\left\{\frac{-\alpha_1}{p}\left(\frac{w_d}{2} - |r|\right)\right\}} \quad \textbf{for} \quad |r| \le \frac{w_d}{2} \\ \mathbf{OAR} &= \mathbf{t + (0.5 - t) * \exp\left\{\frac{-\alpha_2}{p}\left(|r| - \frac{w_d}{2}\right)\right\}} \quad \textbf{for} \quad |r| > \frac{w_d}{2} \end{aligned} , \qquad (3\text{-}1)$$

where α_1 and α_2 are the fit parameters, w_d is the field width defined as the distance between the fifty percent isodose points, r is the radial distance from the center of the field, p is the width of the penumbra, and t is the transmission through the mMLC when all leaves are closed. Transmission was measured by St. John and Wagner and was determined to be 0.7%.[5,7] Meeks also measured transmission; he determined the maximum transmission between leaf sides to be 0.5% and between leaf ends to be

1.2%.[17] The two transmission measurements averaged together agree with St. John's and Wagner's measurements.

The width of the penumbra, defined as the distance between the 80% and 20% isodose points, was measured and determined to be 0.33 mm. A typical example of the Cunningham model, fit to cross-plane data, is shown (Figure 3-1). There are several other functions alternative to the Cunningham model that have been used to fit penumbra profiles.[12, 19] These functions are continuous and have only one fitting parameter, but they don't seem to fit the data as well as the discontinuous Cunningham model. In reality, a continuous function offers no advantage over a discontinuous one because our data points are sampled discretely.

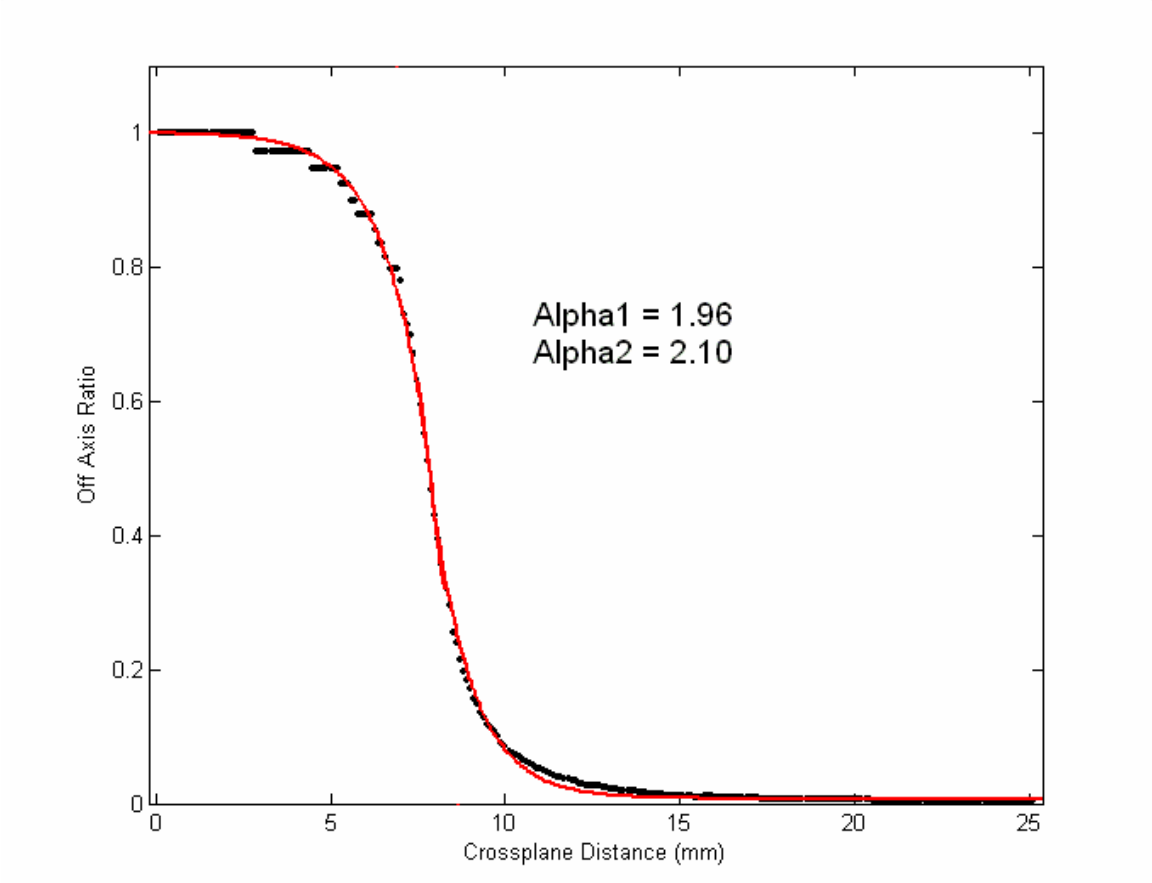

Figure 3-1. Cunningham model fit to cross-plane data from a rectangular field formed by the mMLC. The rectangular field is 18 mm wide.

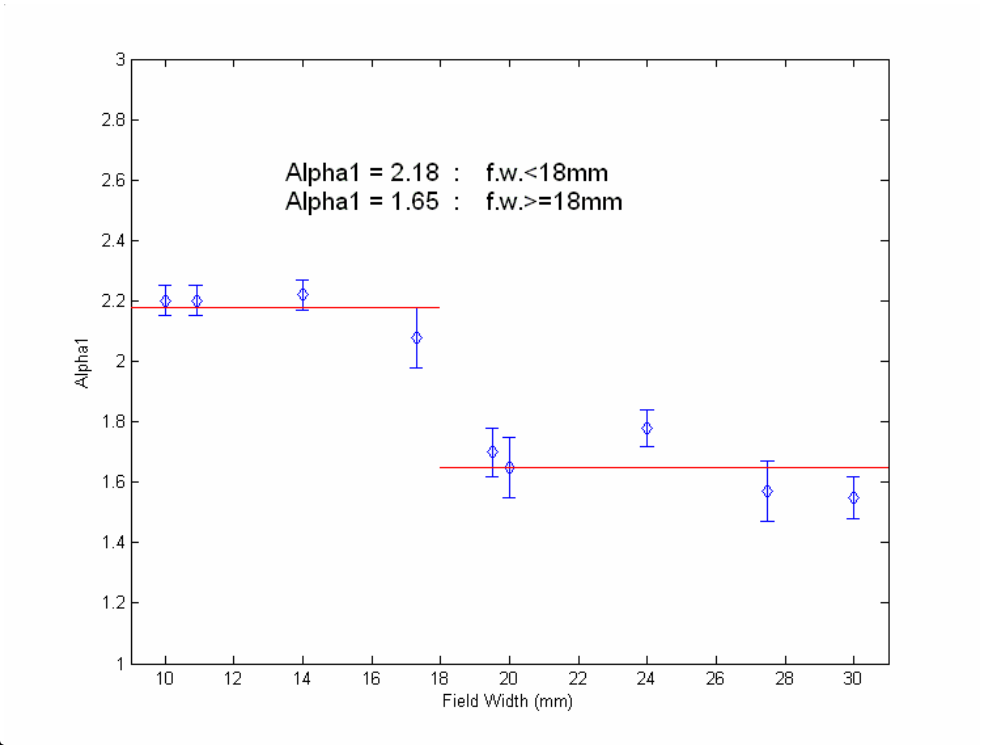

A

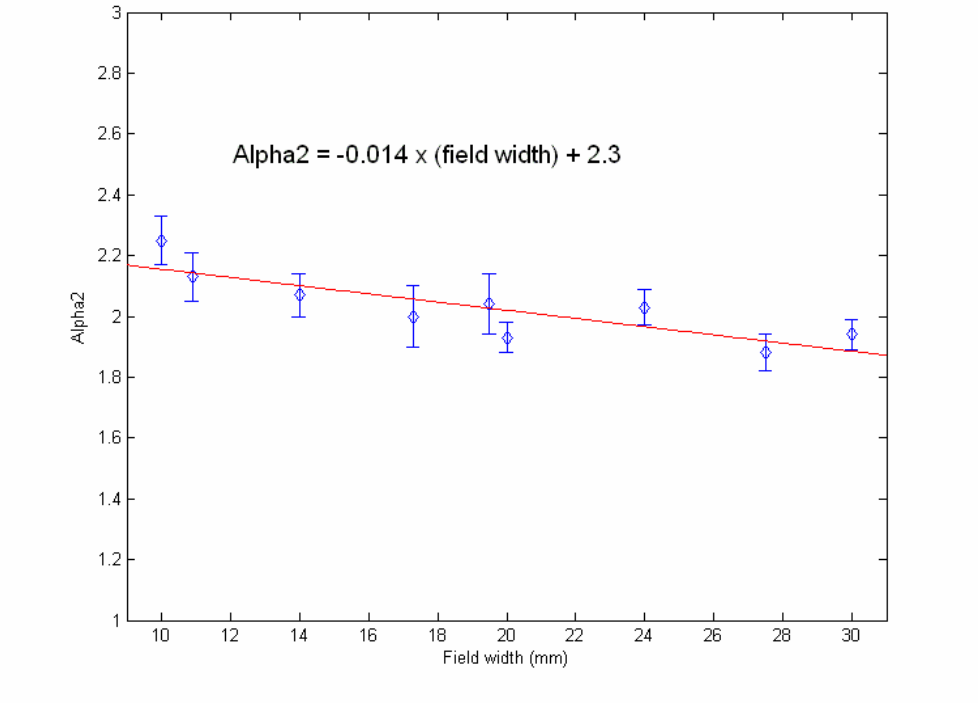

B

Figure 3-2. Plots of the fitting parameters as a function of field width. A) A step function is fit to the α1 parameters. B) A straight line is fit to the α2 parameters. These fits are input into a Matlab program and are used to create models of rectangular fields.

The fitting parameters for each rectangular field were plotted against field width (Figure 3-2). A discontinuity is noted when α_1 is plotted against field width; this discontinuity was also seen by St. John. The discontinuity is the result of adding more open leaves to the field and the field approaching lateral equilibrium. A step function was fit to the calculated α_1 parameters. The plot of the α_2 parameters versus field width is linear, so a straight line was fit to the data.

The fits of the alpha parameters were input into a Matlab program that was developed to produce the final models of the mMLC circular fields. Once the alpha parameter fits are input into the program, the program is able to produce a 2-D model of a rectangular field. When the user enters mMLC leaf positions into the program, the program creates a model of a rectangular field with width equal to the widest open leaf. The length of the field is equal to the product of the number of open leaves in the field and the leaf width. Leaf width is a variable within the program, so the program can be applied to mMLCs of varying leaf widths. Whether or not an odd or even number of leaves is used to approximate the circle is also variable within the program.

After the rectangular field is created, any negative fields that are to be subtracted from the rectangular field are calculated. The size, position, and weight of the negative field had to be considered carefully. If any of these negative field variables were not accurate, the final model would not agree well with measurement. We also had to account for the possibility of overlapping negative fields for cases that required the subtraction of more than one negative field.

The first step in calculating the negative field is to determine the cross-plane profile through the center of the leaf where the first negative field will be placed (Figure 3-4).

The cross-plane profile is derived directly from the rectangular model in the case where only one negative field is applied to the rectangular open field. The total number of negative fields to be applied is equal to the number of open leaves in the quarter field minus one. If more than one negative field is to be applied, the negative field that is calculated first is the largest and is located on the open leaf furthest from the center of the field.

After the cross-plane profile through the rectangular field has been determined, the profile is shifted to match the actual mMLC leaf position for the circular field. For example, in the case of a 22 mm mMLC shaped circle formed with an even number of leaves, the actual positions of the two open leaves in the quarter field are 10.8 mm and 8.7 mm, respectively (Figure 3-3).

After the cross-plane profile through the modeled rectangular field (10.8 mm by 10 mm in the quarter field) has been determined (Figure 3-4), the cross-plane data is shifted back, from 10.8 mm to 8.7 mm to match the position of the second leaf (Figure 3-5). After the cross-plane profile has been shifted, the difference between the rectangular cross-plane profile and shifted cross-plane profile is determined. The result is a profile of the negative field in the cross-plane direction (Figure 3-6). The previous steps are repeated for the in-plane profile; the product of the 1-D negative field cross-plane and in-plane profiles yields a spatial map of the negative field.

In cases where more than one negative field is applied, the negative cross-plane profiles are a weighted combination of cross-plane profiles derived from the rectangular field and the resultant field after the previous negative field was subtracted. This is done so regions of the rectangular field are not subtracted twice by overlapping negative fields.

There is no need to weight the in-plane profiles as such because of the order the negative fields are subtracted. The in-plane profiles are derived directly from the most current version of the model. For example, if one negative field had been subtracted from the rectangular field, the next in-plane profile would be derived from the field that resulted after the subtraction of the first negative field.

Results

The negative field technique was applied to models of rectangular fields to create models of the mMLC shaped circular fields that were measured. Several metrics were used to compare the final, modeled fields, with the measured fields. The first metric is qualitative; it consists of overlapping contour plots of the measured and modeled fields. By visually inspecting this plot, one can quickly determine if the model agrees well with measurement.

The next two metrics provide a means to quantitatively compare the measured and modeled dose distributions. In low gradient regions of the field (regions where the off-axis ratio is not changing rapidly), the error between the modeled and measured fields is best represented by the absolute dose difference between the two fields. In high gradient regions (the penumbra), the dose difference does not provide a good means of quantifying the error. Instead, the error in high gradient regions is represented by the distance between points of equal relative dose. We chose 5% and 1 mm to be the error criteria for our dose-difference and distance-to-agreement tests, respectively.

A program was developed in Matlab to perform error analysis on the modeled fields using the measured fields as the reference. The program determines the dose-difference and distance-to-agreement error for nearly all points in the modeled field. The program then places each error point into either a dose-difference or distance-to-

agreement histogram depending on how well if fit the respective error criteria. The results are two-dimensional histograms of dose-difference and distance-to-agreement error. The level of agreement between the modeled fields and reference fields is observed by these histograms. If all points had less than 1 mm distance-to-agreement error or less than 5% dose-difference error, then the modeled field has met the error criteria. The error analysis program also determines the percentage of error points that have either a dose-difference error less than 3% or distance-to-agreement error less than 0.5 mm.

A third histogram is created to display the dose-difference error and distance-to-agreement error together for all points. It is obvious from inspecting the 3-d histograms that high gradient regions can have a large dose-difference error, but small distance-to-agreement error. And vice versa, low gradient regions can have a large distance-to-agreement error, but small dose-difference error. One can also see from these histograms whether or not the error criteria are met.

The contour plots and histograms show that the modeled even fields agree well with what was measured. All of the even models meet or exceed the error criteria. In fact, at least 96% of the error points lay within 3% dose error or 0.5 mm distance error for the even fields presented in our study.

Discussion

A tool was developed, to model in 2-D, the off-axis ratios of mMLC shaped circular fields, based on a small number of measurements. The tool proved to be fast; it can produce a 2-D off-axis ratio table in less than 1 s. The amount of time necessary to perform measurement and analysis to determine the parameters for input into the tool takes less than half a day. The tool proved to be accurate. All of the modeled fields

shaped with an even number of leaves met the error criteria (5% dose-dose error in low gradient regions and 1 mm distance-to-agreement error in high gradient regions). Many of the models had the majority of its errors be much less than the error criteria. The tool is also flexible. Variables such a leaf width and output size can be readily changed within the program.

Some of the modeled odd fields did not agree well with what was measured. The error is not inherent in the model. It was determined that some of the leaves on the mMLC were not properly aligned when the odd field measurements were made. This effect caused the actual leaf positions to be different from the specified leaf positions by about 0.7 mm on average.

To check leaf alignment, some leaf pairs of interest were opened individually and made to project 2 cm wide at isocenter. The physical distance between the leaves were measured with a micrometer and projected to isocenter. The results of these measurements (Table 3-1) show the leaves were not properly aligned. Leaf alignment was performed about a week before the even field measurements were made. Odd field measurements were performed over six months later; it is quite possible that leaf position accuracy was affected over this time period. Sastre-Padro et al. performed stability and reproducibility measurements on an MLC and reported a maximum leaf shift of 0.27 mm over three months.[20]

Table 3-1. Leaf alignment check

Leaf Pair[a]	Physical Separation (mm)	Length Projected to Isocenter[b] (mm)	Absolute Error (mm)
8	12.68 ± 0.05	19.51 ± 0.08	0.49
9	12.39 ± 0.05	19.06 ± 0.08	0.94
10	12.05 ± 0.05	18.54 ± 0.08	1.46
11	12.18 ± 0.05	18.74 ± 0.08	1.26
12	12.60 ± 0.05	19.38 ± 0.08	0.62
13	12.71 ± 0.05	19.55 ± 0.08	0.45

[a]Each leaf pair was opened individually and the distance between them was measured with a micrometer. [b]The length projected to isocenter should be 20 mm.

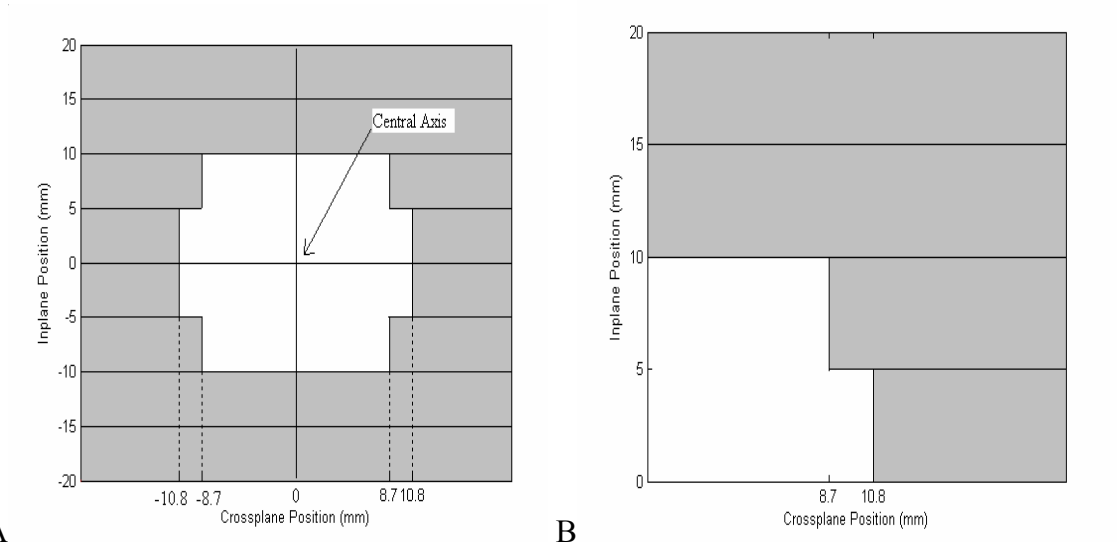

A B

Figure 3-3. The mMLC leaf positions for a 22 mm circular approximation with even leaves. A) All leaves in the open field are shown. B) The leaves in the quarter field are shown. Because of symmetry, it is necessary to model only a quarter of the field.

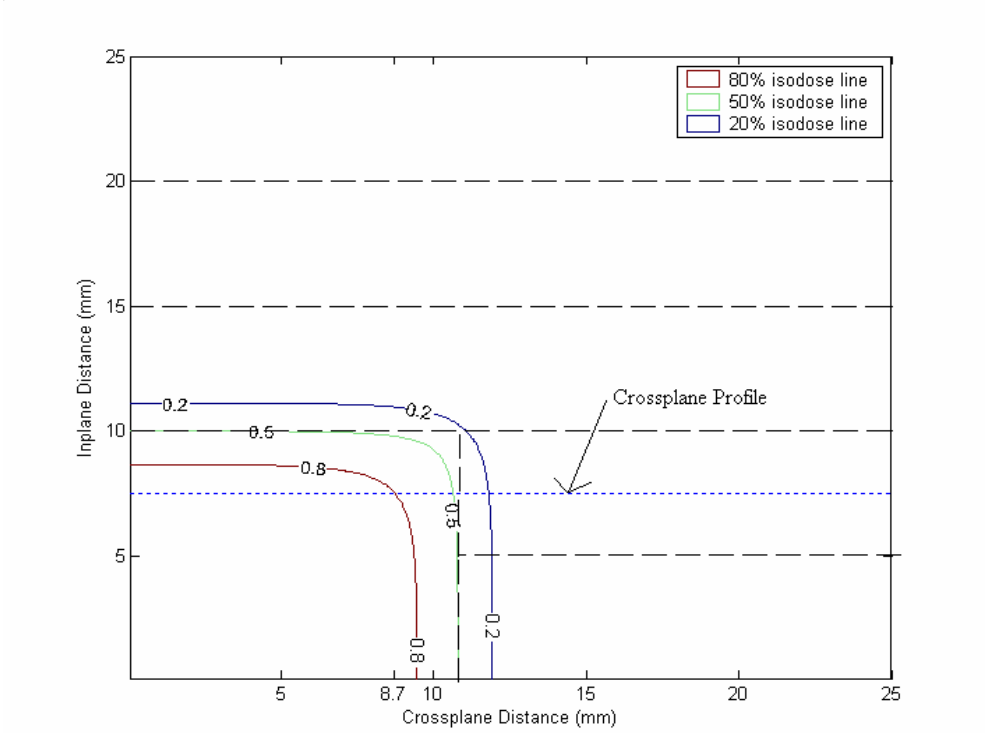

A

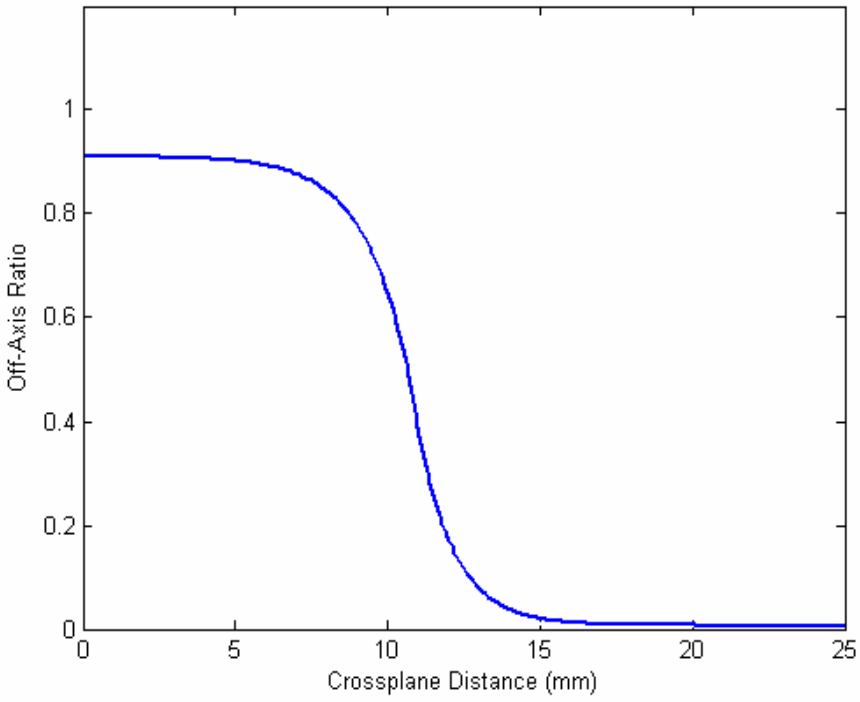

B

Figure 3-4. A cross-plane profile through the rectangular open field is determined. A) A contour plot of the rectangular field. The black dashed lines are the hypothetical mMLC leaf positions for the rectangular model. B) The derived cross-plane profile.

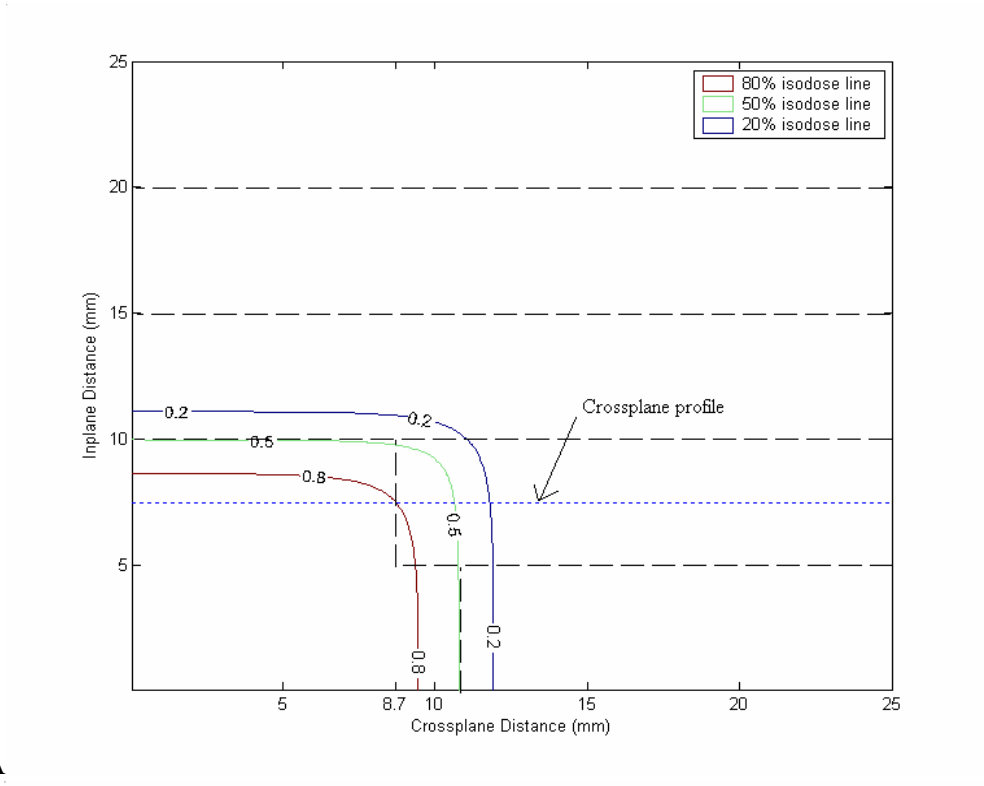

A

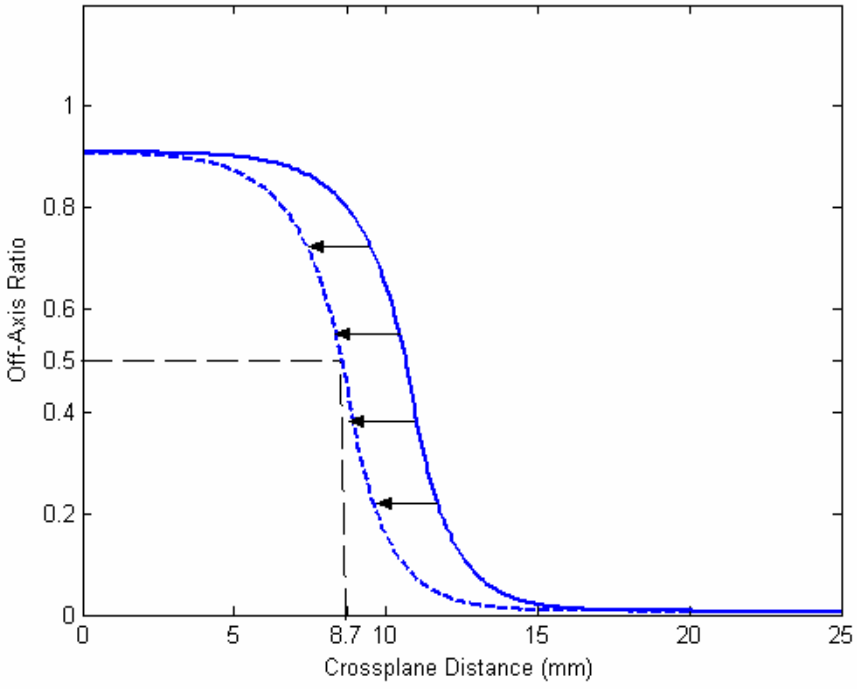

B

Figure 3-5. The cross-plane profile is shifted to match the position of the mMLC leaf. A) Contour plot of the rectangular field and actual mMLC leaf positions for a 22 mm circular field. B) The cross-plane profile before and after the shift.

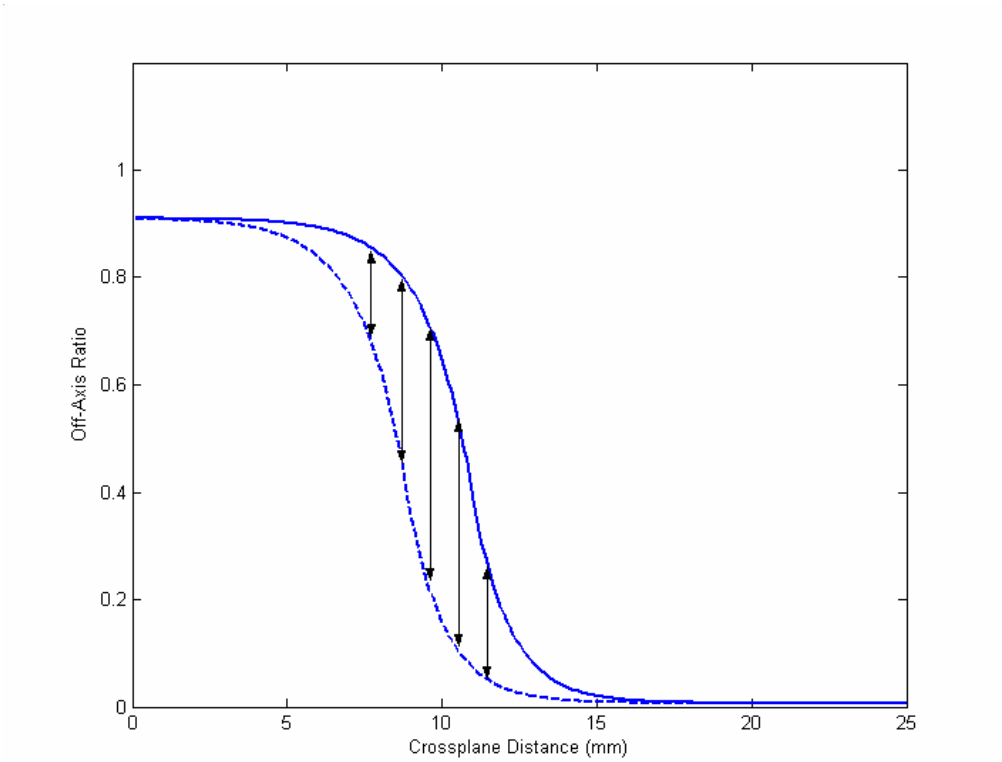

A

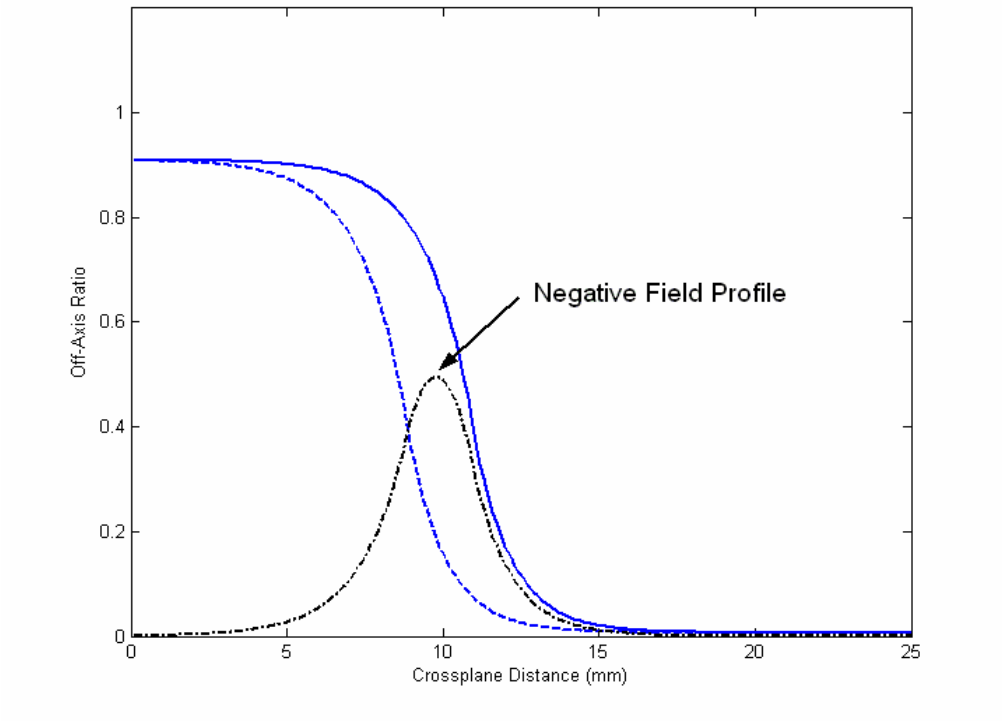

B

Figure 3-6. Negative field profile. A) The difference between the cross-plane profiles is determined. B) The resulting cross-plane profile of the negative field is shown.

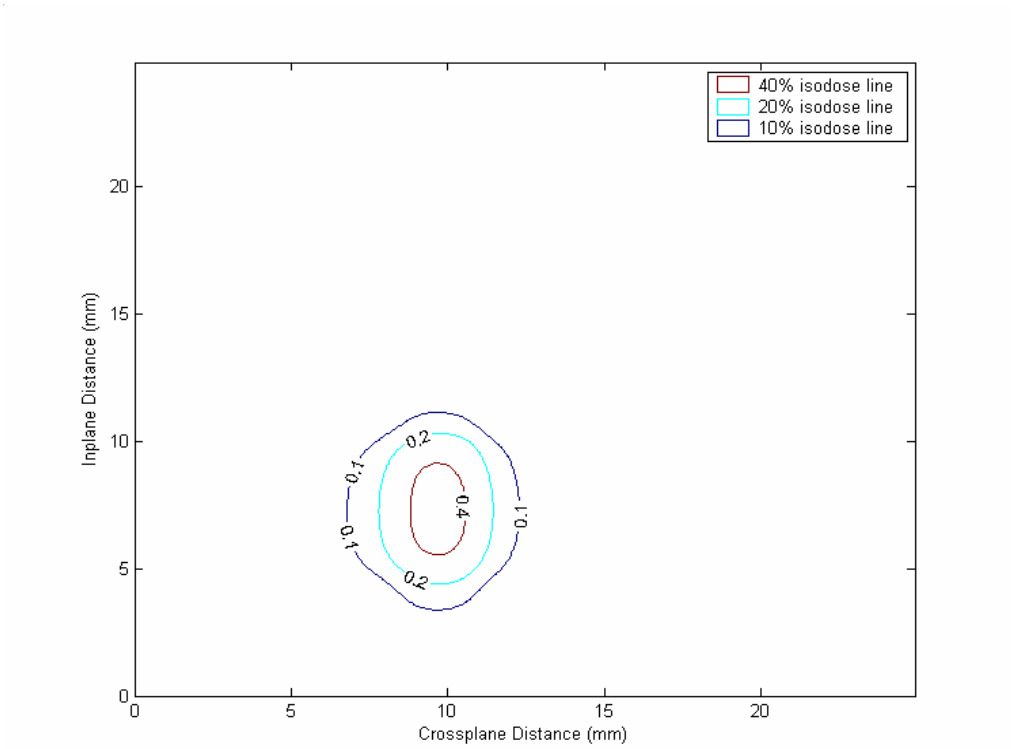

A

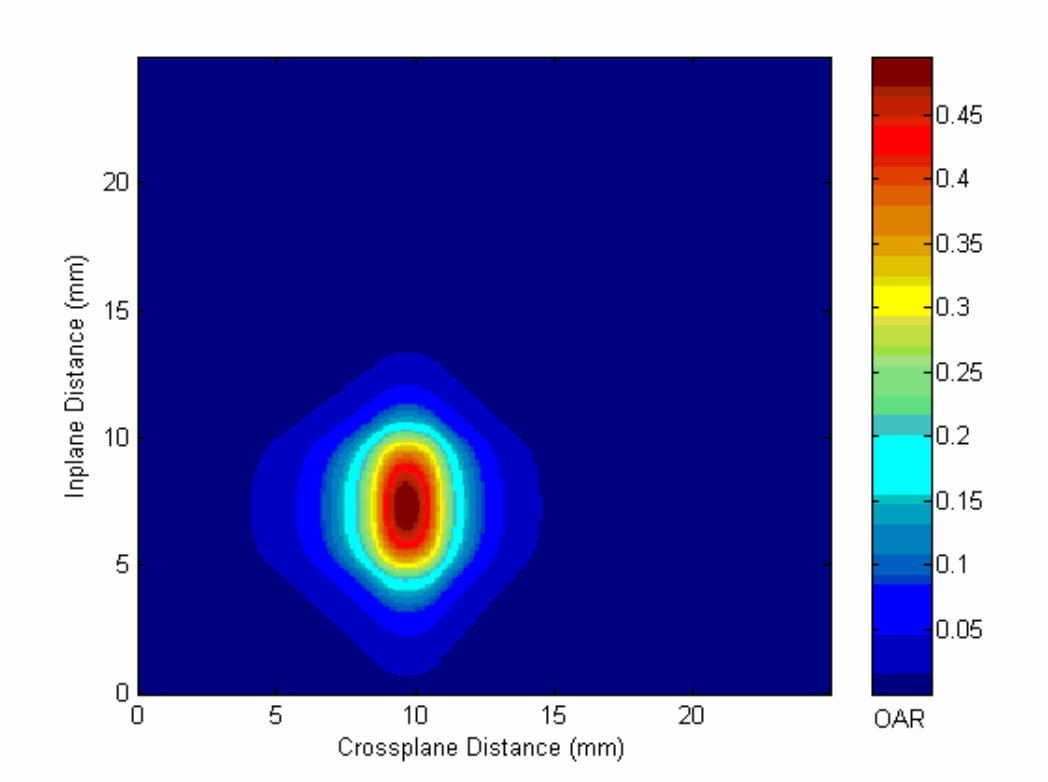

B

Figure 3-7. Spatial map of negative field. A) A contour plot of the negative field. B) A color-wash plot. The negative field is applied to a rectangular field to produce the final model of a 22 mm mMLC circular approximation.

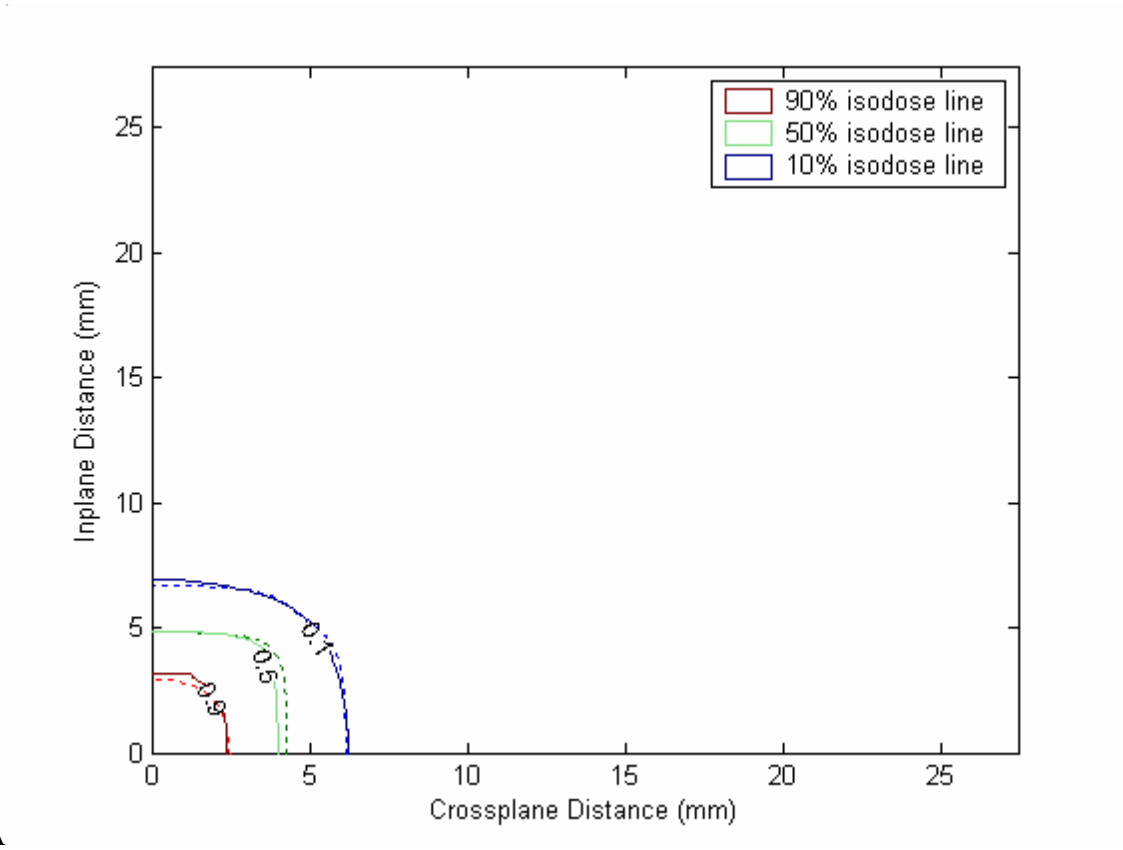

A

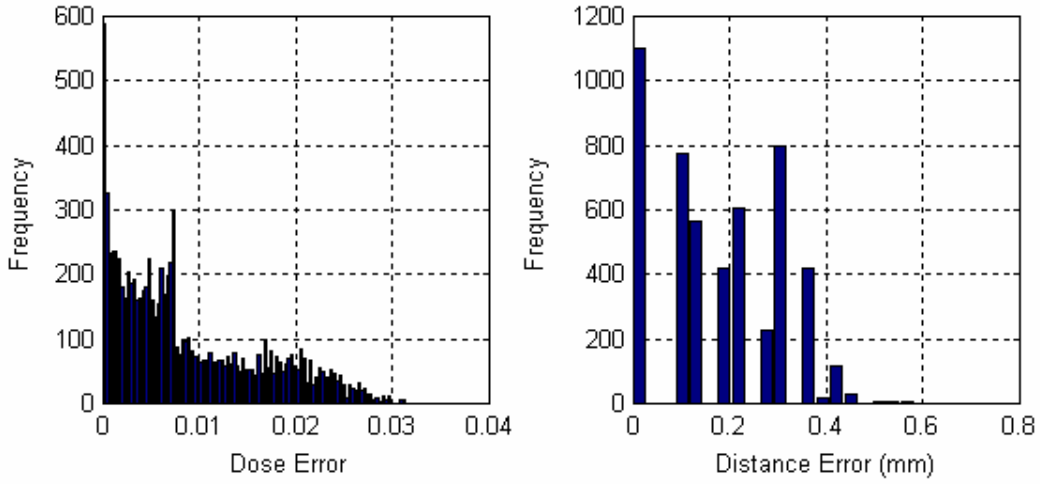

B

Figure 3-8. A 10 mm mMLC circular field formed by an even number of leaves.
A) Contour plots of measured (solid line) and modeled (dashed line) fields.
B) Histograms of dose-difference error and distance-to-agreement error comparing the modeled field to the reference measured field.
C) Three-dimensional histogram of distance error and percent error. All points have either dose error less than 3.25% or distance error less than 0.6 mm.

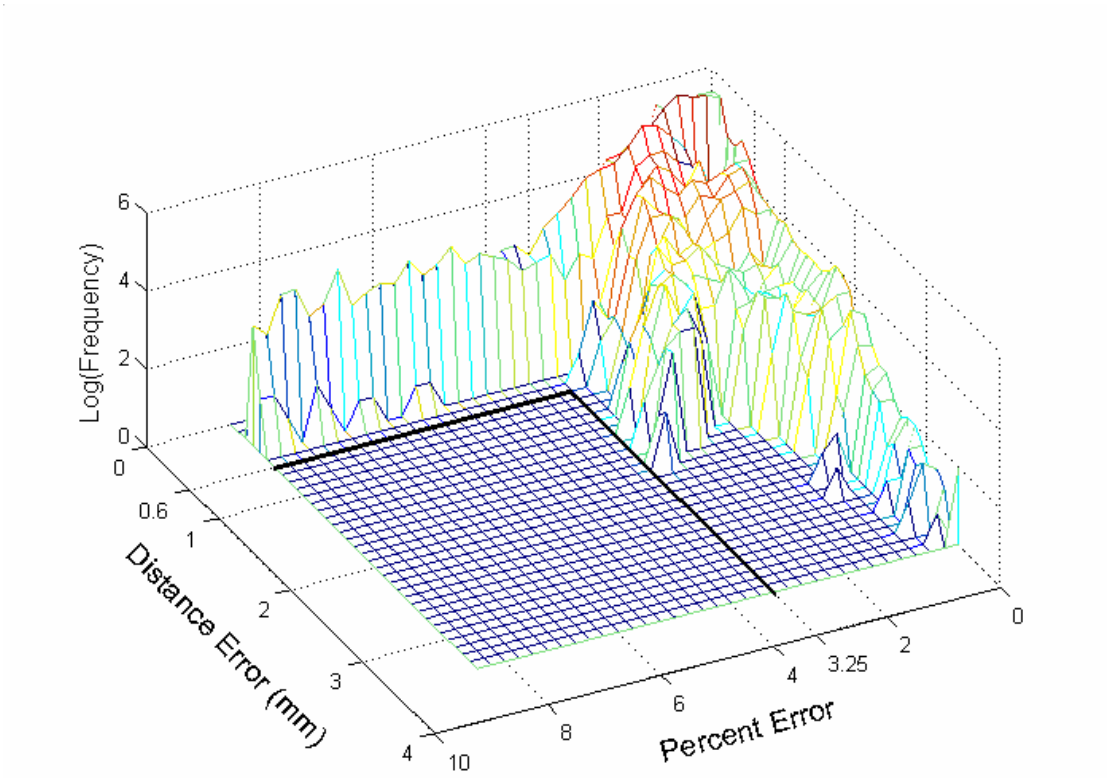

C

Figure 3-8. Continued

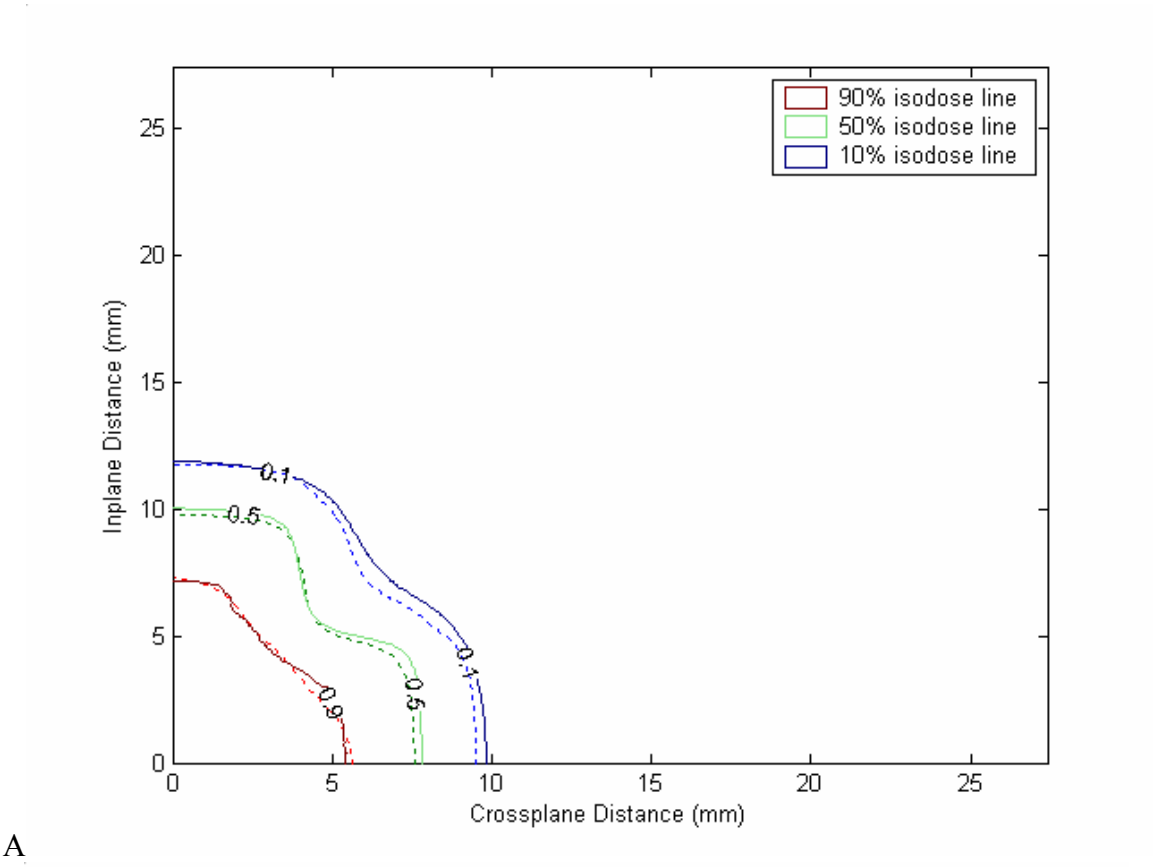

A

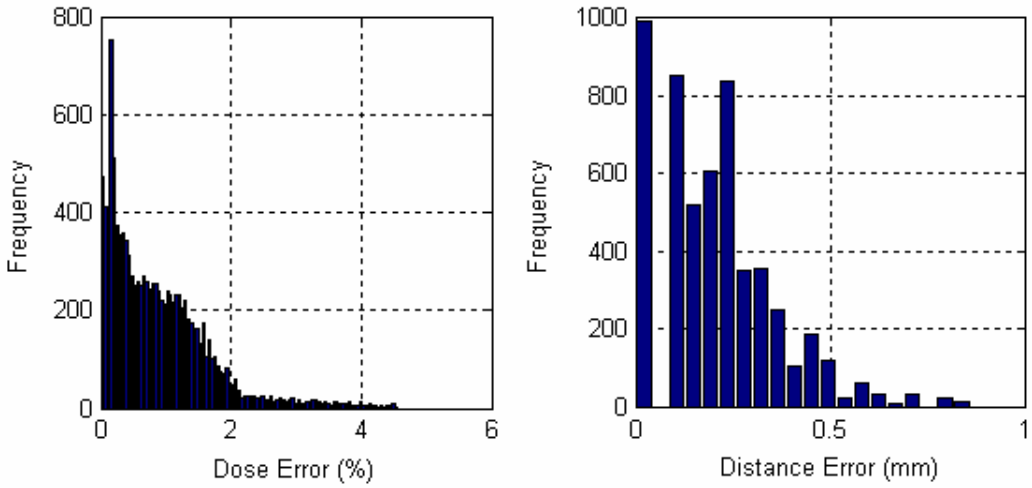

B

Figure 3-9. A 16 mm mMLC circular field formed by an even number of leaves.
A) Contour plots of measured (solid line) and modeled (dashed line) fields.
B) Histograms of dose-difference error and distance-to-agreement error comparing the modeled field to the reference measured field.
C) Three-dimensional histogram of distance error and percent error. All points have either dose error less than 4.7% or distance error less than 0.9 mm.

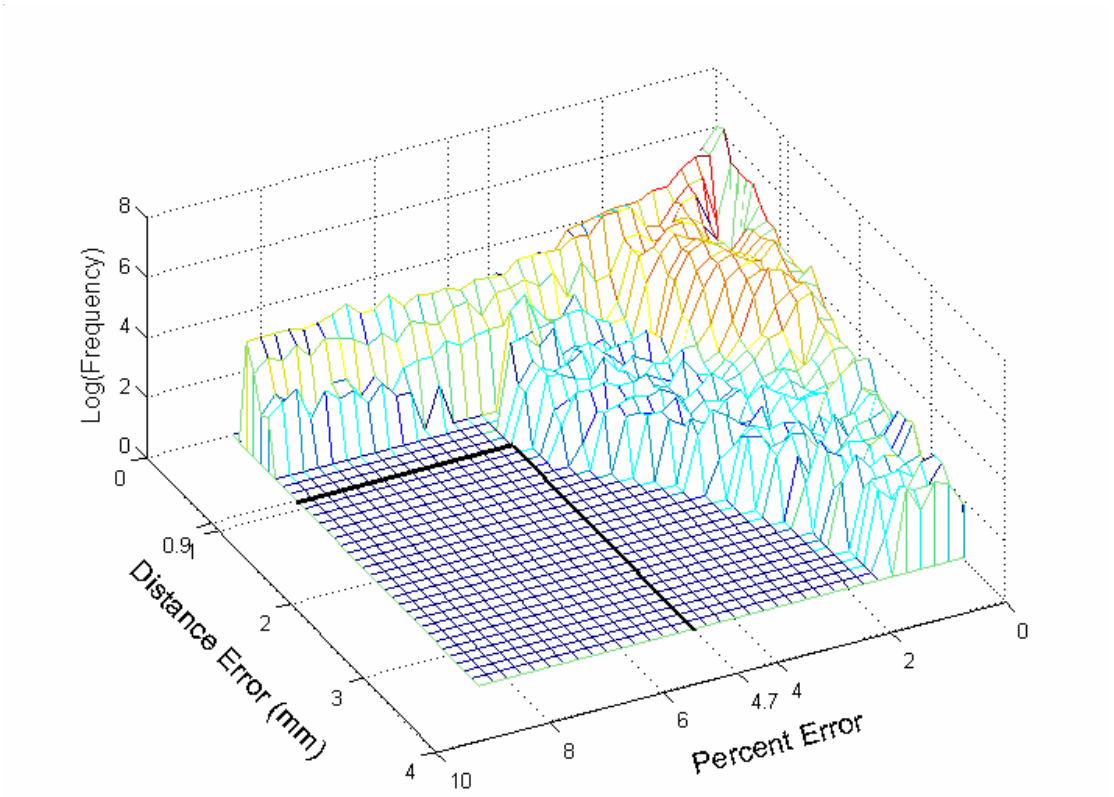

C

Figure 3-9. Continued

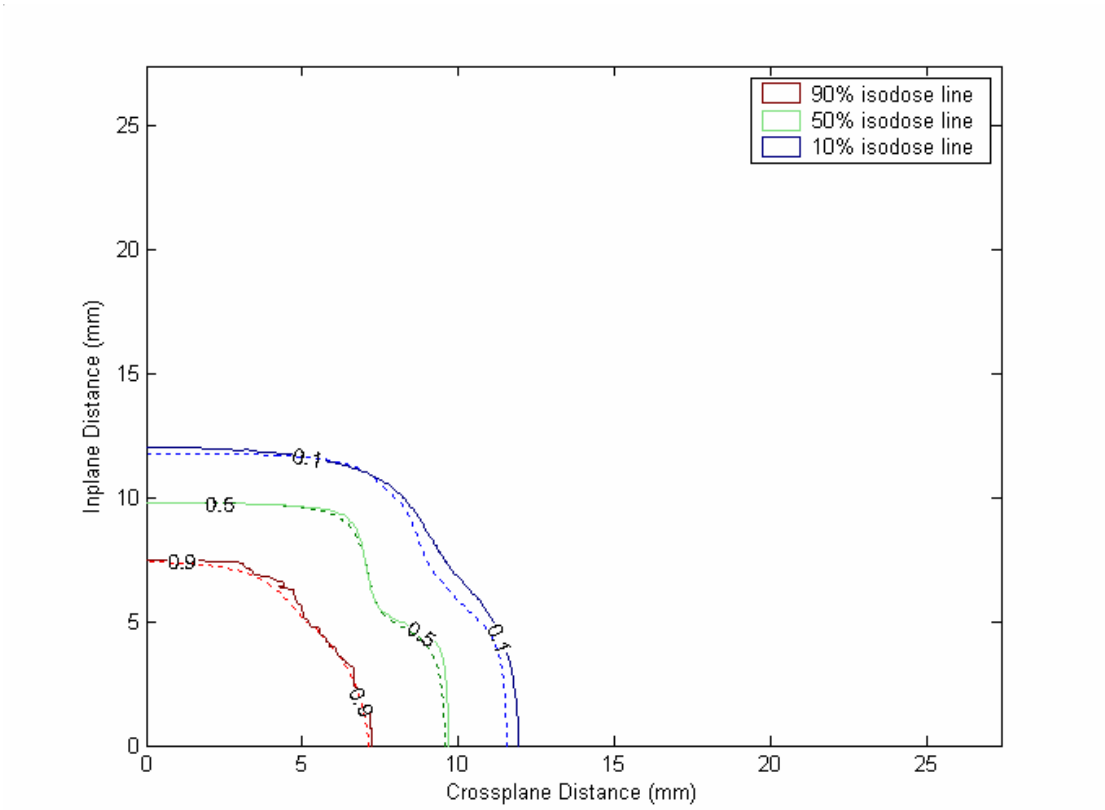

A

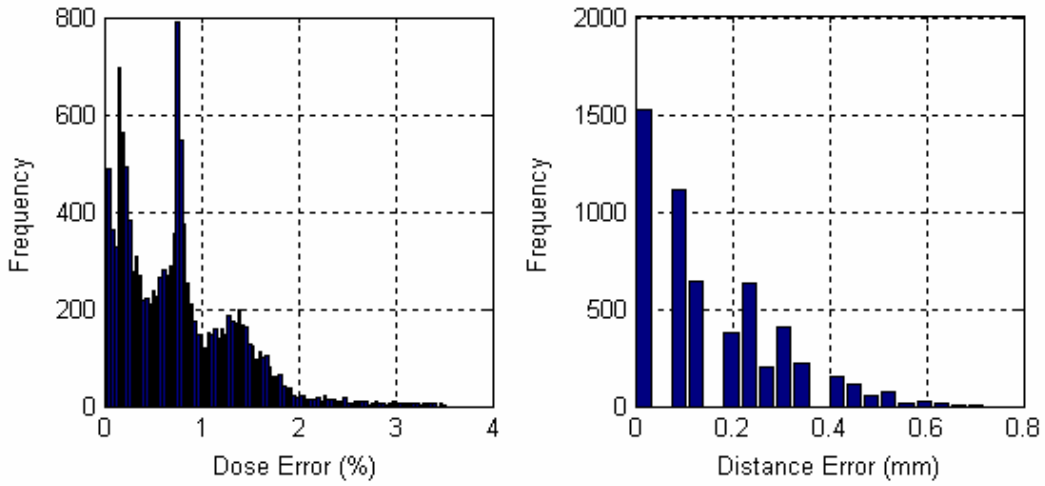

B

Figure 3-10. A 20 mm mMLC circular field formed by an even number of leaves.
A) Contour plots of measured (solid line) and modeled (dashed line) fields.
B) Histograms of dose-difference error and distance-to-agreement error comparing the modeled field to the reference measured field.
C) Three-dimensional histogram of distance error and percent error. All points have either dose error less than 3.5% or distance error less than 0.75 mm.

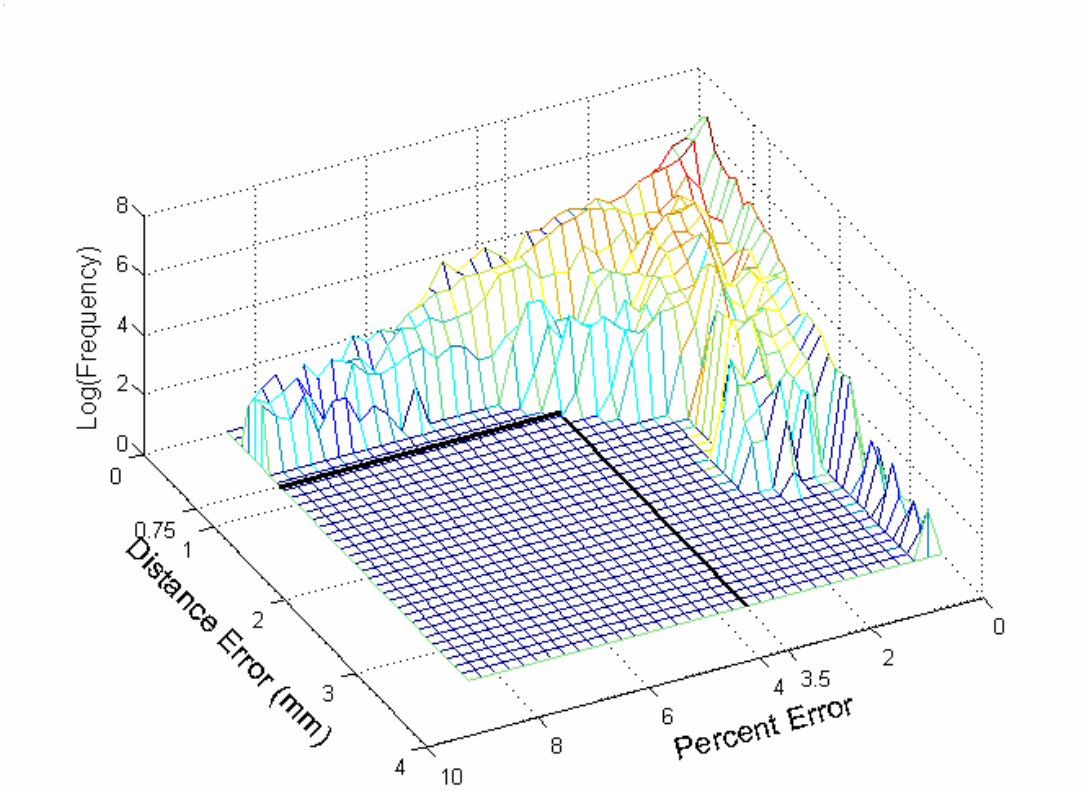

C

Figure 3-10. Continued

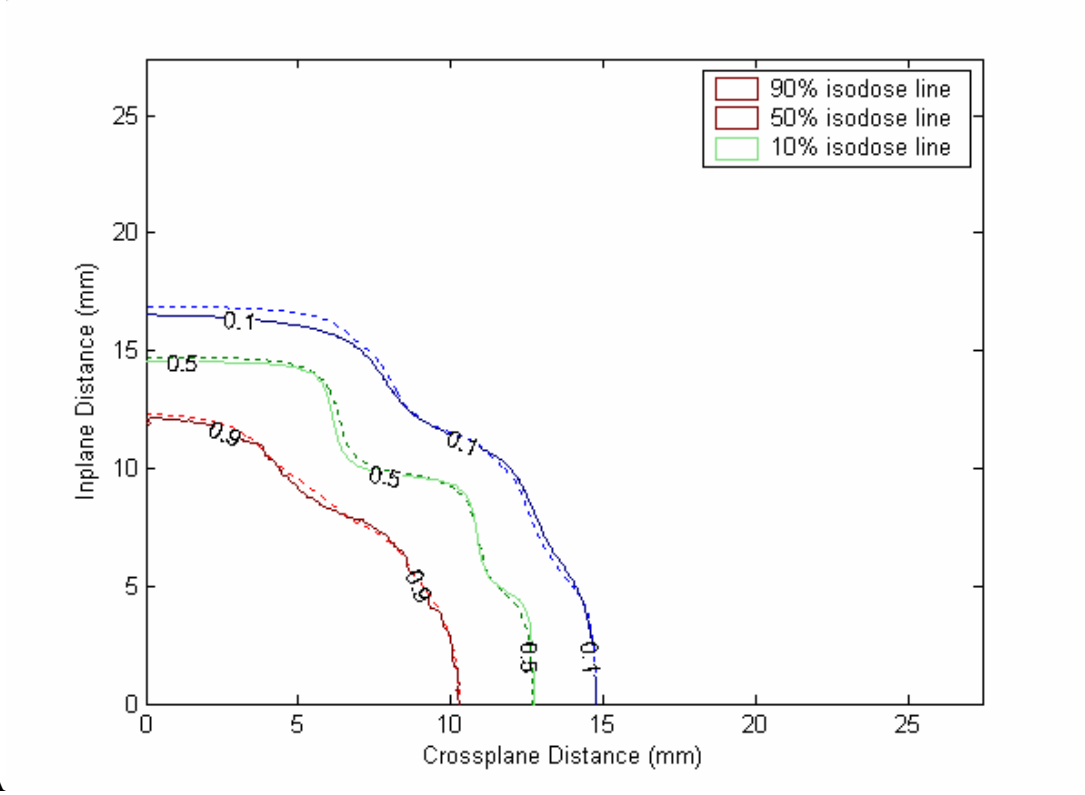

A

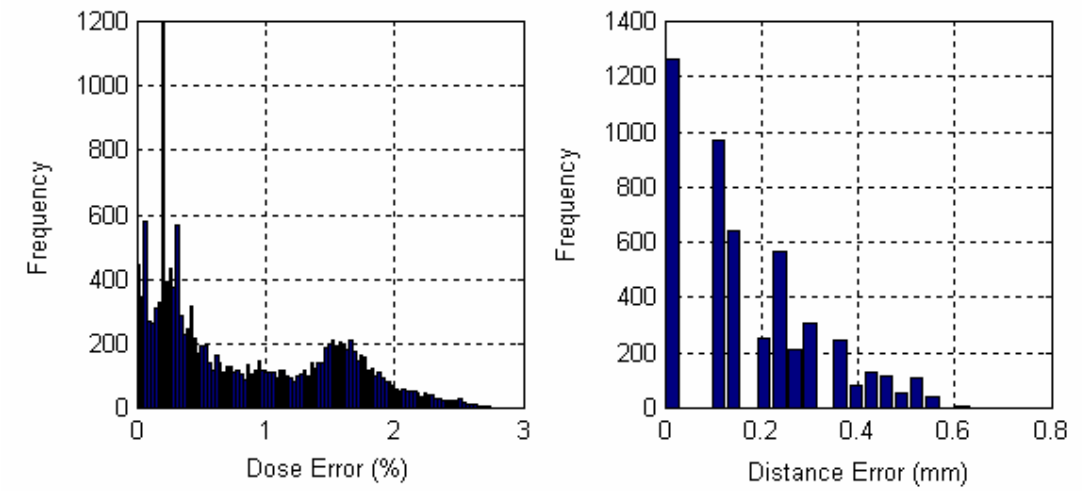

B

Figure 3-11. A 26 mm mMLC circular field formed by an even number of leaves. A) Contour plots of measured (solid line) and modeled (dashed line) fields. B) Histograms of dose-difference error and distance-to-agreement error comparing the modeled field to the reference measured field. C) Three-dimensional histogram of distance error and percent error. All points have either dose error less than 2.8% or distance error less than 0.7 mm.

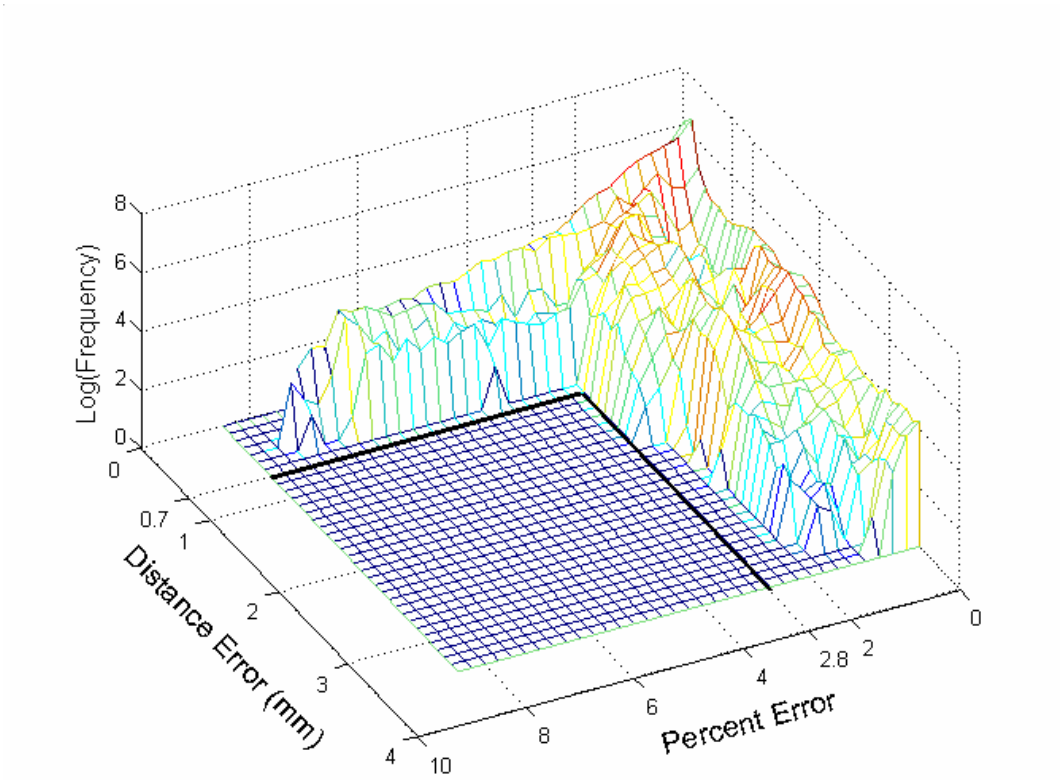

C

Figure 3-11. Continued

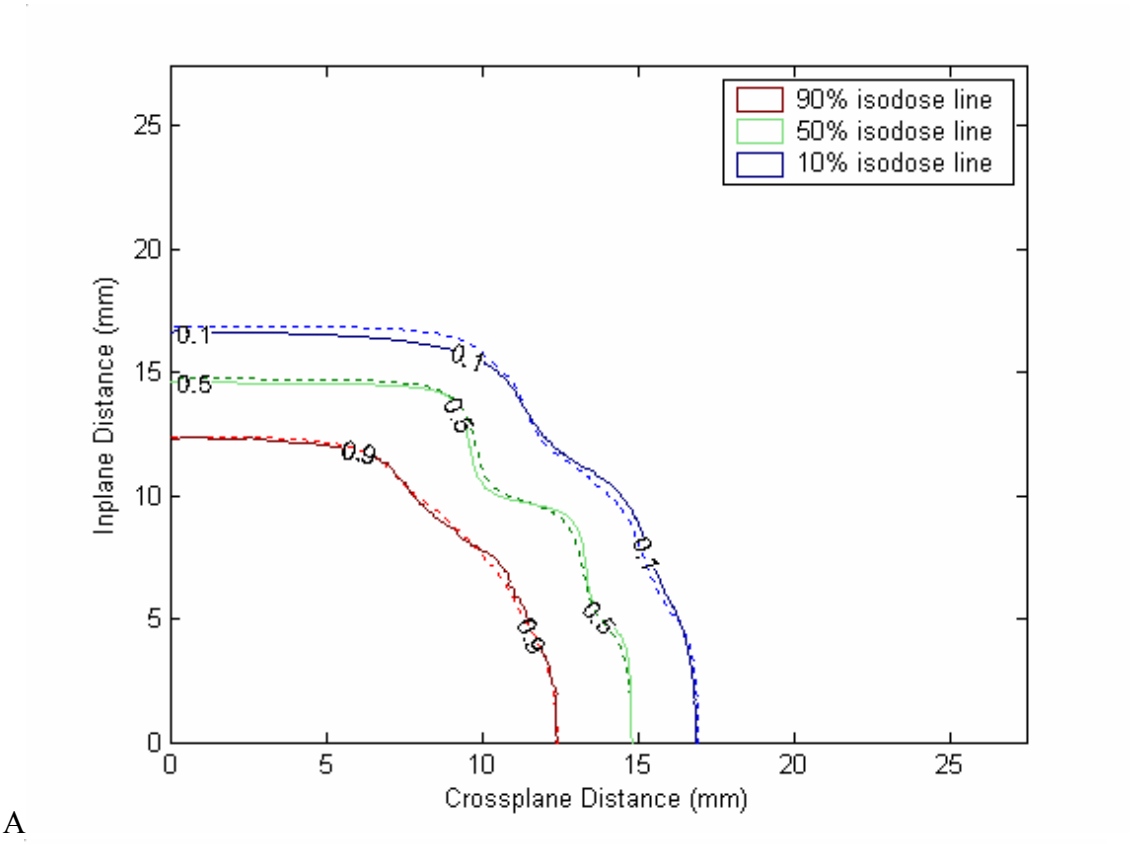

A

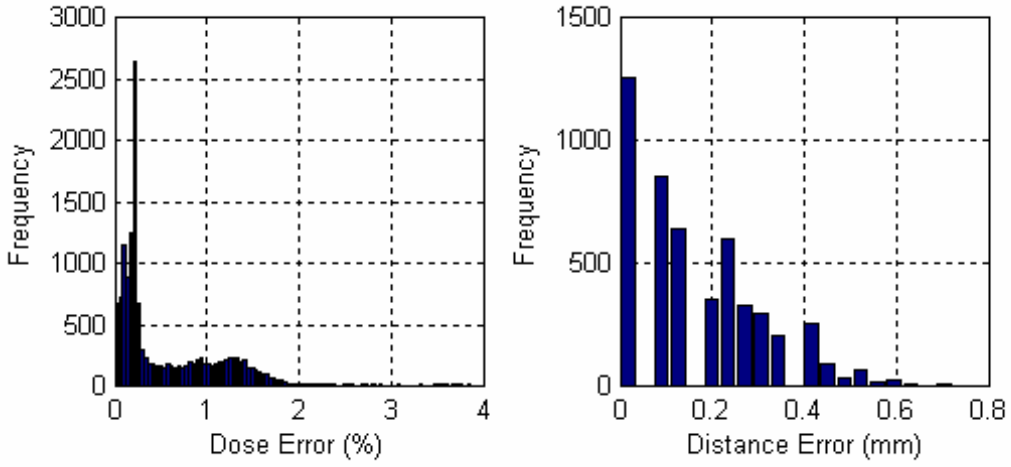

B

Figure 3-12. A 30 mm mMLC circular field formed by an even number of leaves.
A) Contour plots of measured (solid line) and modeled (dashed line) fields.
B) Histograms of dose-difference error and distance-to-agreement error comparing the modeled field to the reference measured field.
C) Three-dimensional histogram of distance error and percent error. All points have either dose error less than 4% or distance error less than 0.8 mm.

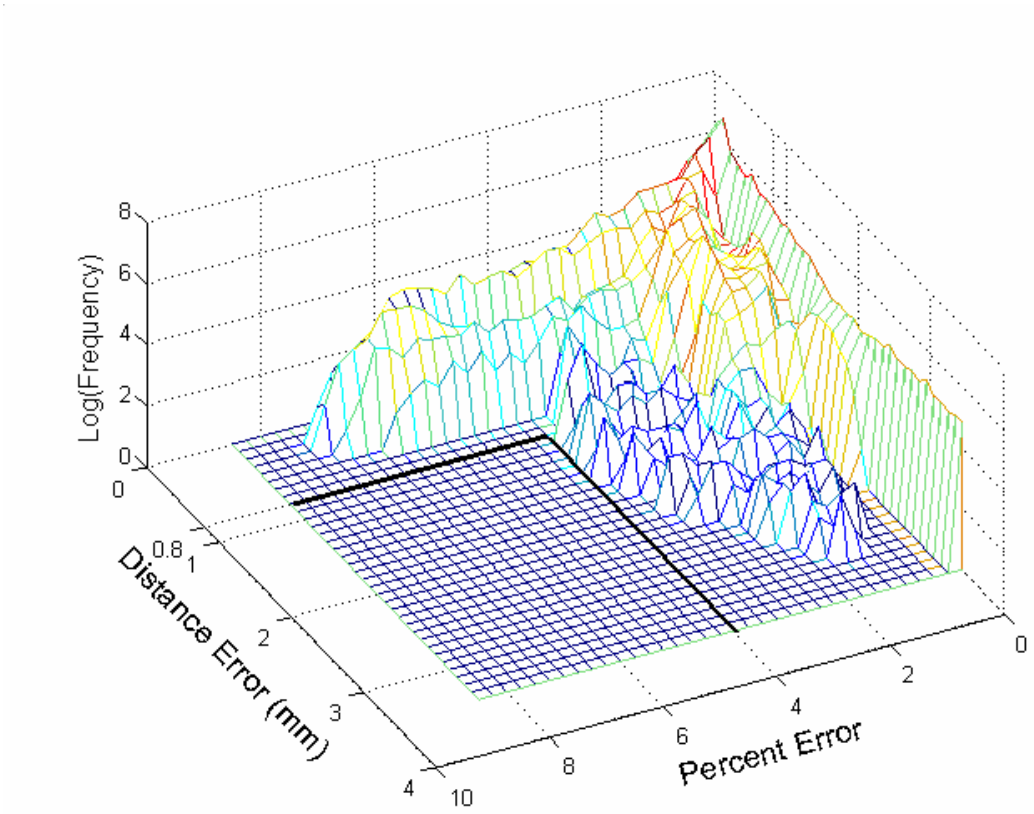

C

Figure 3-12. Continued

CHAPTER 4
CONCLUSION

The work presented in this report tackled the problem of how to produce two dimensional off-axis ratio tables for circular fields approximated by a mini-multileaf collimator. The use of a mMLC in conjunction with the multiple isocenter delivery technique will allow for more efficient treatment delivery and increased patient satisfaction while maintaining conformal dose distributions with steep dose gradients.

Two methods for producing the tables of OARs were investigated. The first method was direct measurement of the fields with radiographic film. This method proved to be rather tedious and time consuming because many films needed to be exposed, processed, and analyzed. The second method investigated was an empirical one based on the negative field technique. A tool was developed in the Matlab programming environment to create models of the mMLC circular fields based on the negative field technique where negative fluences are applied to an open field to achieve the desired dose distribution. The program requires the user to input several OAR fitting parameters that can be quickly obtained from a small number of measurements. Once the fitting parameters are input into the program, the program will output a spatial map of off-axis ratios for any specified mMLC shaped circular field.

The modeled fields produced by the program were compared to the fields measured with radiographic film. A tool was developed to perform error analysis on the modeled fields with respect to a reference (measured) field. This was accomplished by determining the dose-difference error in low gradient regions of the field and distance-to-

agreement error in high gradient regions of the field. More than 90% of points in the modeled even fields had dose-difference error less than 3% or distance-to-agreement error less than 0.5 mm. The modeled odd fields did not agree as well with measurement because the mMLC leaves were not moving to the specified location when the measurements were made. It should be noted from this experience that the leaves on the mMLC must be properly aligned and their positions accurately known for this method to work properly. Overall, the tool proved to be fast, flexible, easy to use, and accurate.

Future work will include showing that the model can be applied to fields located off-axis and at different depths. It is expected that the model will work fine in these situations because it has been shown that the penumbra of small fields does not change much with depth or off-axis position. Future work on the tool used to create the modeled fields will include having the tool be able to model any field shaped by the mMLC, as opposed to just being able to model circular fields.

APPENDIX A
MATLAB PROGRAM DEVELOPED TO MODEL THE FIELDS

```
msgbox('Select command window and enter inputs');

numleaf=input('Enter the number of leaves in the quarter field (default=1):');
if isempty(numleaf)
  numleaf=1;
end

for i=1:numleaf
   prompt = sprintf('Enter the position of leaf %d in mm:  ',i);
   leafpos(i)=input(prompt);
end

%////////////////////////////////////////////////////////////////////////
%THESE VARIABLES MAY BE CHANGED TO ACCOMODATE DIFFERENT MLC, ODD OR
EVEN
%FIELDS, ETC

%EVEN OR ODD NUMBER OF LEAVES (1 FOR EVEN, 0 FOR ODD)
even = 1;

%LEAF WIDTH (mm)
lfwidth = 4.95 %5.0;

scale = 0.1;  %(mm/pixel)

%SIZE OF RESULING MATRIX  (mm)
sizematrix = 27.5;
pixels = sizematrix/scale;
%////////////////////////////////////////////////////////////////////////

w1 = leafpos(1)*2; %FIELD LENGTH

%FIELD WIDTH
if even==1     %EVEN CASE
   w2 = lfwidth * numleaf * 2;
else
   %ODD CASE
   w2 = lfwidth * (numleaf *2 -1);
end

%////////////////////////////////////////////////////////////////
%These are the fit parameters for the rectangular fields.
%THESE PARAMETERS CAN BE MODIFIED FOR A PARTICULAR MLC/LINAC
COMBINATION

if w1<18
   alpha1cross = 2.18;
```

```
else
   alpha1cross = 1.65;
end
if w2<18
   alpha1in = 2.18;
else
   alpha1in = 1.65;
end
alpha2cross = -.0135*w1+2.29;
alpha2in = -.0135*w2+2.29;

%////////////////////////////////////////////////////////////////////

t=.0075; %TRANSMISSION CONSTANT
p=2.4;   %PENUMBRA CONSTANT

%Produce Square Field ////////////////////////////////////////////////////////
matrx=zeros(pixels,pixels);
for i=1:pixels
   m=scale*i;
   if m<(w1/2)
      crossratio(i)=(1-.5*exp(-alpha1cross*(w1/2-m)/p));
   else
      crossratio(i)=(t+(.5-t)*exp(-alpha2cross*(m-(w1/2))/p));
   end
end

for i=1:pixels
   m=scale*i;
   if m<(w2/2)
      inratio(i)=(1-.5*exp(-alpha1in*(w2/2-m)/p));
   else
      inratio(i)=(t+(.5-t)*exp(-alpha2in*(m-(w2/2))/p));
   end
end

matrx=zeros(pixels,pixels);
l=1;
for i=1:pixels
   k=1;
   for j=1:pixels
      matrx(i,j)=crossratio(k)*inratio(l);
      k=k+1;
   end
   l=l+1;
end
newmatrx=matrx;
%////////////////////////////////////////////////////////////////////////

%////////////////////////////////////////////////////////////////////////
%BEGIN CALCULATING AND SUBTRACTING NEGATIVE FIELDS

for q=(numleaf-1):-1:1  %NUMLEAF-1 IS THE NUMBER OF NEGATIVE FIELDS

   centerx = round((leafpos(q+1) + (leafpos(1)-leafpos(q+1))/2)*10);
   if even==1
```

```
    centery = (q+.5)*lfwidth*10;  %EVEN CASE
 else
    centery = q*lfwidth*10;       %ODD CASE
 end
 centery=round(centery);

    w1= leafpos(q+1);
if even==1     %EVEN CASE
  w2new = lfwidth*(q) * 2;
 else
    %ODD CASE
    w2new = 2* lfwidth * (q-.5);
 end

centery=round(centery);
 square=newmatrx(centery,:);
 norm=max(square);
 for i=1:pixels
    m=scale*i;
    if m<(leafpos(q+1))
       newcross(i)=norm*(1-.5*exp(-alpha1cross*(w1-m)/p));
    else
       newcross(i)=norm*(t+(.5-t)*exp(-alpha2cross*(m-w1)/p));
    end
 end

 square2=newmatrx(:,centerx);
 norm2=max(square2);
 for i=1:pixels
    m=scale*i;
    if m<(w2new/2)
       newin(i)=norm2*(1-.5*exp(-alpha1in*(w2new/2-m)/p));
    else
       newin(i)=norm2*(t+(.5-t)*exp(-alpha2in*(m-(w2new/2))/p));
    end
 end

  if q==(numleaf-1)       %DONT WEIGHT FIRST NEGATIVE FIELD

    end1=pixels;
    for i=1:end1

       pt1 = newmatrx(centery,i);
       pt2= newcross(i);
       if (pt1-pt2)>0
          negcross(i)=pt1-pt2;
       else
          negcross(i)=0;
       end
    end
 else                  %WEIGHT OTHER NEGATIVE FIELDS
    end1=pixels;
    for i=1:end1

       wt1=(2*centerx-i+1)/(2*centerx);
       wt2= i/(2*centerx);
```

```
        pta=newmatrx(centery,i);
        ptb=matrx(centery,i);
        pt1 = wt2*pta+wt1*ptb;
        pt2= newcross(i);
        if (pt1-pt2)>0
            negcross(i)=pt1-pt2;
        else
            negcross(i)=0;
        end
    end
end

    negin=zeros(1,pixels);
    for i=1:pixels

        pt1 =newmatrx(i,centerx);
        pt2= newin(i);
       if (pt1-pt2)>0
            negin(i)=pt1-pt2;
       else
            negin(i)=0;
       end

    end

max1=max(negin);
max2=max(negcross);
if max1>max2
   avemax=max1;
else
   avemax=max2;
end

[z,end2]=size(negin);
negmatrx=zeros(end2,end1);
l=1;
for i=1:end2
    k=1;
    for j=1:end1
        negmatrx(i,j)=(negcross(k)*negin(l))/avemax;
        k=k+1;
    end
    l=l+1;
end

if q==2
    neg1=negmatrx;
else
    neg2=negmatrx;
end

for i=1:end2
    for j=1:end1
        newmatrx(i,j)=newmatrx(i,j)-negmatrx(i,j);
    end
end
```

```
end

X=(0:(pixels-1)).*scale;

figure
 [C,h] = contour(X,X,newmatrx,[.9 .5 .1],':');hold on;
 %[C,h] = contour(X,X,odd28mm,[.9 .5 .1]); clabel(C,h);
 Xlabel('Crossplane Distance (mm)');
 Ylabel('Inplane Distance (mm)');
 legend(h,'90% isodose line','50% isodose line','10% isodose line');
```

APPENDIX B
MATLAB PROGRAM DEVELOPED TO PERFORM ERROR ANALYSIS ON MODELED FIELDS

```
clear X X1 finaldist finaldose gammadose gammadist histomatrix;

%TYPE THE NAME OF THE REFERENCE DOSE PROFILE IN THE WORKSPACE
refdose = even30;

fieldwidth=23;  %max 23
lngthofr=(fieldwidth/2)+10;

numpix=275;

k=1;
t=1;
z=1;
%CHECK EACH PIXEL VALUE FOR DOSE-DOSE ERROR

      for theta = 0: 0.017 : pi/2

         for r = 0: 0.1 : lngthofr
            r2=r*10;
            y = round(r2 *sin(theta)) +1;
            x = round(r2 *cos(theta)) +1;

            dose_err(k)=abs(newmatrx(y,x)-refdose(y,x));

            match=refdose(y,x);         %REFERENCE VALUE FOR DOSE WE WANT TO FIND
DISTANCE TO

            if r<4
               start=0;
            else
               start=r2-40;
            end

            for r3=start:0.5:(r2+45)
               y2 = round(r3 *sin(theta)) +1;
               x2 = round(r3 *cos(theta)) +1;
               temp=newmatrx(y2,x2);
               if temp<=match
                  dist(k)=sqrt((y2-y)^2+(x2-x)^2)*.1;
                  break
               else
                  dist(k)=4.5;
               end
            end

            gammadist=dist(k)/1;
```

```
        gammadose=dose_err(k)/0.05;

        if gammadose<gammadist
           finaldose(t)=dose_err(k);
           t=t+1;
        else
           finaldist(z)=dist(k);
           z=z+1;
        end

        k=k+1;

    end
end

dose_err=dose_err.*100;
%CREATE 2-D PLOT OF BINNED ERRORS
prcntbin=0.25;
distbin=0.1;

rndprcnt=prcntbin/2;
rnddist=distbin/2;

[m,n]=size(dist);

histomatrix=zeros(50,40);
lghistomatrix=zeros(50,40);

for i=1:n
    temp1=dist(i);
    temp2=dose_err(i);

    temp1=temp1+rnddist;
    temp2=temp2+rndprcnt;

    temp1=round(temp1/distbin);
    temp2=round(temp2/prcntbin);

    if temp2<40
        histomatrix(temp1,temp2)=histomatrix(temp1,temp2)+1;
    end
end

 [m,n]=size(histomatrix);
for i=1:m
    for j=1:n
        if histomatrix(i,j)~=0
            temp = histomatrix(i,j);
            lghistomatrix(i,j)=log(temp);

        end
    end
end

%DETERMINE THE RATIO OF PTS THAT HAVE LESS THAN .5mm DISTANCE ERROR
%OR 3% DOSE ERROR.
```

```
      cnt=0;
    sumhisto=sum(sum(histomatrix));
    for i=1:m
       for j=1:n
          if (i<6)|(j<13)
          cnt=cnt+histomatrix(i,j);

          end
       end
    end
    ratio=(cnt/sumhisto)*100

    distaxes=(0:distbin:(distbin*(m-1)));
    prcntaxes=(0:prcntbin:(prcntbin*(n-1)));

    meshz(prcntaxes(1,1:35),distaxes(1,1:35),lghistomatrix(1:35,1:35));
    xlabel('Percent Error','Rotation',15,'Fontsize',14);
    ylabel('Distance Error (mm)','Rotation',-45,'Fontsize',14);
    zlabel('Log(Frequency)','Fontsize',12);
    set(gca,'zscale','linear');view(153,54);

figure

N=zeros(100,1);
        [N,X]=hist(finaldose,100);

P=zeros(20,1);
  [P,X1]=hist(finaldist,20);

  subplot(1,2,1)
bar(X*100,N); grid on; Xlabel('Dose Error (%)'); Ylabel('Frequency');
pbaspect([1 1 1]);%Title('Histogram');
subplot(1,2,2)
bar(X1,P); grid on; Xlabel(' Distance Error (mm)'); Ylabel('Frequency');
pbaspect([1 1 1]);%Title('Histogram');
```

APPENDIX C
MATLAB PROGRAM DEVELOPED TO ANALYZE A CALIBRATION FILM

```
function calib_separate

%CALIB_SEPARATE
% This function opens calibration tiff files, selected by operator, one at a time
% and plots a histogram of optical density. By clicking on the background peak
% and exposure peak for each file, a dose calibration curve is calculated.
% Coefficients a, b, & c are returned for the equation dose = a*OD^2 + b*OD + c.

msgbox('Select command window and enter inputs');

num=input('Enter the number of calibration exposures (default=8):');
if isempty(num)
  num=8;
end
output=input('Enter the output factor (default=1.0):');
if isempty(output)
  output=1;
end
MU(1,1)=0;
for i=1:num
  prompt=sprintf('Enter MUs for exposure # %d:  ',i);
  MU(i+1,1)=input(prompt);
end

OD=zeros(num+1,1);

dose=MU.*output
%film_type=input('Enter the film type(XV or EDR),(default{XV}):');
%if isempty(film_type)
%   film_type='XV';
%end
%film_type

for j=1:num
  prompt=sprintf('Select file number %d',j)
  [scanfile,direc]=uigetfile('*.tif',prompt);

  if scanfile==0
    return;
  end

cd(direc);
fid1=fopen(scanfile);

if fid1 ~=-1
        raw=imread(scanfile,'tif');
else
```

```
  msgbox('File not found\n');
  return;
end

if j==1
  f1=figure;
  set(f1,'position',[120 40 600 480]);
end
[A,B]=size(raw);
raw2=double(raw);

for i=1:A
   for z=1:B
      if raw2(i,z)==0
         raw2(i,z)=1;
      end
   end
end

raw2=-log10(raw2/255);  %Convert to OD

N=zeros(500,1);
% HIST(raw) creates a matrix with histograms of each column in the matrix(raw)
[N1,X]=hist(raw2,500);
% Combine all histograms into a single histogram (X contains bin centers)
for i=1:B
  N(:,1)=N(:,1) + N1(:,i);
end

M = max(max(raw2)); %Use M to set axis limits
Mn=max(max(N));
% Draw the plots
p1 = subplot(2,2,1);imagesc(raw),colormap gray, axis square;Title('Raw Image');
p2 = subplot(2,2,2); plot(0,0)
p3 = subplot(2,1,2);
%[N,X]=hist(raw1,50);hist(raw1(25,:),50);hold on
bar(X,N); grid on; Xlabel('Optical Density'); Ylabel('Frequency');
h1=uicontrol('style','text','position',[100 230 400 20 ],'BackgroundColor','w');
set(h1,'string','****Click on BACKGROUND peak****');
[X,Y]=ginput(1);
BKGpts(j)=X;
set(p3,'xlim',[0 M],'ylim',[0 Mn]);pbaspect([2 1 1]);
set(h1,'string','****Click on Exposure peak****');
[X,Y]=ginput(1);
ODpoint(j)=X;
% Leave row 1 col 1 for zero dose

OD(j+1)=ODpoint(j);
delete(h1);
end
BKGpts
BKG=mean(BKGpts);
%std(BKGpts(:,1))/BKG;            % = standard deviation
OD(1)=BKG;
OD;
dose;
```

```
for t=1:num+1
   OD(t)=OD(t)-BKG;
end
OD
dose
OD_size=size(OD)
dose_size=size(dose);
dose=output.*MU;
Mdose=max(dose);
MaxOD=max(OD);

%******
facts=polyfit(OD,dose,2);
a=facts(1);
b=facts(2);
c=facts(3);
for i=1:(MaxOD)*50
  dose_fit(i,1)=a*(i/50)^2 + b*(i/50) + c;
  Xaxis(i)=i/50;
end
dose_fit;
%*****linear fit
%facts=polyfit(OD(2:6),dose(2:6),1);
%a=0;
%b=facts(1);
%c=facts(2);
%for i=1:num
%   dose_fit(i,1)=b*OD(i,1) + c;
%end
axes(p2);
cla
plot(Xaxis,dose_fit,'color','r','LineWidth',2);

%plot(dose_fit,OD/1000,'color','r','LineWidth',2);
hold on;

plot(OD(1:num+1),dose(1:num+1),'*');grid on;
YLabel('Dose (cGy)');XLabel('Optical density (OD)');Title('Calibration Curve (BKG-corrected)');

% Write the fitting parameters at the bottom of the plot

h1=uicontrol('style','text','position',[60 225 500 20 ],'BackgroundColor','w');

result=sprintf('The calibration curve is Dose = %7.3e*OD^2 + %7.3e*OD + %4.3f ',a,b,c);
set(h1,'ForeGroundColor','r','FontWeight','Bold','string',result);

% Write calibration factors
fid=fopen('calib.info','w');
fprintf(fid,'Calibration film: %s\n',pwd);
fprintf(fid,'%7.3e \t %7.4f \t %7.4f\n',a,b,c);
fprintf(fid,'%7.4f',BKG);
set(findobj('tag','cal_a'),'string',a);
set(findobj('tag','cal_b'),'string',b);
set(findobj('tag','cal_c'),'string',c);
fclose(fid);
```

```
% write dose and OD to file for Excel
fid=fopen('plot3.txt','w');
for i=0:num-1
   j=num-i;
   fprintf(fid,'%f\t%f\n',OD(j),dose(j));
end

fclose(fid);
```

APPENDIX D
MATLAB PROGRAM DEVELOPED TO SEPARATE AND ALIGN EXPOSURES

```
function varargout = separate_exp(varargin)
% SEPARATE_EXP M-file for separate_exp.fig
%      SEPARATE_EXP, by itself, creates a new SEPARATE_EXP or raises the existing
%      singleton*.
%
%      H = SEPARATE_EXP returns the handle to a new SEPARATE_EXP or the handle to
%      the existing singleton*.
%
%      SEPARATE_EXP('CALLBACK',hObject,eventData,handles,...) calls the local
%      function named CALLBACK in SEPARATE_EXP.M with the given input arguments.
%
%      SEPARATE_EXP('Property','Value',...) creates a new SEPARATE_EXP or raises the
%      existing singleton*.  Starting from the left, property value pairs are
%      applied to the GUI before separate_exp_OpeningFunction gets called.  An
%      unrecognized property name or invalid value makes property application
%      stop.  All inputs are passed to separate_exp_OpeningFcn via varargin.
%
%      *See GUI Options on GUIDE's Tools menu.  Choose "GUI allows only one
%      instance to run (singleton)".
%
% See also: GUIDE, GUIDATA, GUIHANDLES

% Edit the above text to modify the response to help separate_exp

% Last Modified by GUIDE v2.5 22-Feb-2005 05:11:31

% Begin initialization code - DO NOT EDIT
gui_Singleton = 1;
gui_State = struct('gui_Name',       mfilename, ...
                   'gui_Singleton',  gui_Singleton, ...
                   'gui_OpeningFcn', @separate_exp_OpeningFcn, ...
                   'gui_OutputFcn',  @separate_exp_OutputFcn, ...
                   'gui_LayoutFcn',  [] , ...
                   'gui_Callback',   []);
if nargin & isstr(varargin{1})
   gui_State.gui_Callback = str2func(varargin{1});
end

if nargout
   [varargout{1:nargout}] = gui_mainfcn(gui_State, varargin{:});
else
   gui_mainfcn(gui_State, varargin{:});
end
% End initialization code - DO NOT EDIT

% --- Executes just before separate_exp is made visible.
function separate_exp_OpeningFcn(hObject, eventdata, handles, varargin)
```

```
% This function has no output args, see OutputFcn.
% hObject    handle to figure
% eventdata  reserved - to be defined in a future version of MATLAB
% handles    structure with handles and user data (see GUIDATA)
% varargin   command line arguments to separate_exp (see VARARGIN)

% Choose default command line output for separate_exp
handles.output = hObject;

% Update handles structure
guidata(hObject, handles);
set(hObject,'MenuBar','figure');

% UIWAIT makes separate_exp wait for user response (see UIRESUME)
% uiwait(handles.figure1);

% --- Outputs from this function are returned to the command line.
function varargout = separate_exp_OutputFcn(hObject, eventdata, handles)
% varargout  cell array for returning output args (see VARARGOUT);
% hObject    handle to figure
% eventdata  reserved - to be defined in a future version of MATLAB
% handles    structure with handles and user data (see GUIDATA)

% Get default command line output from handles structure
varargout{1} = handles.output;

% --- Executes during object creation, after setting all properties.
function numexp_CreateFcn(hObject, eventdata, handles)
% hObject    handle to numexp (see GCBO)
% eventdata  reserved - to be defined in a future version of MATLAB
% handles    empty - handles not created until after all CreateFcns called

% Hint: popupmenu controls usually have a white background on Windows.
%       See ISPC and COMPUTER.
if ispc
   set(hObject,'BackgroundColor','white');
else
   set(hObject,'BackgroundColor',get(0,'defaultUicontrolBackgroundColor'));
end

% --- Executes on selection change in numexp.
function numexp_Callback(hObject, eventdata, handles)
% hObject    handle to numexp (see GCBO)
% eventdata  reserved - to be defined in a future version of MATLAB
% handles    structure with handles and user data (see GUIDATA)

% Hints: contents = get(hObject,'String') returns numexp contents as cell array

% --- Executes on button press in getfile.
function getfile_Callback(hObject, eventdata, handles)
% hObject    handle to getfile (see GCBO)
% eventdata  reserved - to be defined in a future version of MATLAB
% handles    structure with handles and user data (see GUIDATA)

num=get(handles.numexp,'Value');    %returns selected item from numexp
scale=str2double(get(handles.scale,'String')); %returns contents of scale as a double
```

```
numpixel=floor(85/scale);  %was 55
check=rem(numpixel,2);      %force number of pixels to be even for ease of calculations
if check==0
else
   numpixel=numpixel+1;
end

[scanfile,direc]=uigetfile('*.tif','Select image' );
cd(direc);
fid1=fopen(scanfile);
if fid1 ~=-1
           I=imread(scanfile,'tif');

else
  fprintf('File not found\n');
  return;
end
cla;

uiwait(msgbox('Box in each exposure.  Hold shift key for square.','modal'));

for i=1:num
   cla;
   axes(handles.image)

   %Allows the user to separate different exposures
    newimage=imcrop(I);

   %Check to see if user wants to center and align exposures
   num2=get(handles.align,'Value');

   if num2==1

      cla;
      contimage=double(newimage);

      imagesc(contimage),colormap gray, axis equal, axis tight;

      uiwait(msgbox('Zoom in and click on each fiducial starting at the top and working
clockwise.','modal'));

      for z=1:4
         k=20;
         zoom on;
        k=waitforbuttonpress;

        if k==0
            [x(z),y(z)]=(ginput(1));
         end
        zoom out;
      end

      %Determine the equations for the lines for the central axis
      m1=(y(2)-y(4))/(x(2)-x(4));
      b1=y(2)-m1*x(2);
```

```
        if x(3)==x(1)  %so don't divide by zero
           xint=round(x(3))
           m2=inf;
        else
            m2=(y(3)-y(1))/(x(3)-x(1));
            b2=(y(3)-m2*x(3));

            %Determine intersection (center of beam)
            xint=round((b2-b1)/(m1-m2));
        end
        yint=round(m1*xint+b1);

%         %if odd
%            yint=yint-25;
%            %end
%
        %Crop the image so the center of beam is center of image
        [A,B]=size(newimage);

        if ((xint<(B/2))&(yint>(A/2))) % first quadrant
            if xint>(A-yint)
               I2=imcrop(newimage,[xint-(A-yint),2*yint-A,2*(A-yint),2*(A-yint)]); % closer to upper half
            else
               I2=imcrop(newimage,[1,yint-xint,2*xint,2*xint]); % closer to left edge...xmin set to 1
instead of 0 b/c dimensions work out that way.
            end
        elseif ((xint<(B/2))&(yint<(A/2))) % third quadrant
            if xint>yint
               I2=imcrop(newimage,[xint-yint,1,2*yint,2*yint]);
            else
               I2=imcrop(newimage,[1,yint-xint,2*xint,2*xint]);
            end
        elseif ((xint>(B/2))&(yint>(A/2))) % second quadrant
            if ((B-xint)<(A-yint))
               I2=imcrop(newimage,[2*xint-B,yint-(B-xint),2*(B-xint),2*(B-xint)]);
            else
               I2=imcrop(newimage,[xint-(A-yint),2*yint-A,2*(A-yint),2*(A-yint)]);
            end
        else % fourth quadrant
            if yint<(B-xint)
               I2=imcrop(newimage,[xint-yint,1,2*yint,2*yint]);
            else
               I2=imcrop(newimage,[2*xint-B,yint-(B-xint),2*(B-xint),2*(B-xint)]);
            end
        end

        %Next, determine how much the image needs to be rotated

         [A,B]=size(I2);
        X=A/(2*m2)+A/2;
       angle=rad2deg(atan(2*X/A-1));
        angle

        %Now rotate the image
        I3=imrotate(I2,-angle,'bicubic','crop');
       cla;
```

```
      [A,B]=size(I3);
      A=A/2-numpixel/2;
      B=B/2-numpixel/2;
      I4=imcrop(I3,[B,A,numpixel-1,numpixel-1]);

      newdirec=strcat(direc,'exposure');
       num2=num2str(i);
       newdirec=strcat(newdirec,num2);
       newdirec=strcat(newdirec,'.tif');

       %Write each separate exposure to a file
       imwrite(I4,newdirec,'tif');

   else
      newdirec=strcat(direc,'exposure');
      num2=num2str(i);
      newdirec=strcat(newdirec,num2);
      newdirec=strcat(newdirec,'.tif');

      %Write each separate exposure to a file
      imwrite(newimage,newdirec,'tif');
   end
%
end
cla;

% --- Executes during object creation, after setting all properties.
function scale_CreateFcn(hObject, eventdata, handles)
% hObject    handle to scale (see GCBO)
% eventdata  reserved - to be defined in a future version of MATLAB
% handles    empty - handles not created until after all CreateFcns called

% Hint: edit controls usually have a white background on Windows.
%       See ISPC and COMPUTER.
if ispc
   set(hObject,'BackgroundColor','white');
else
   set(hObject,'BackgroundColor',get(0,'defaultUicontrolBackgroundColor'));
end

function scale_Callback(hObject, eventdata, handles)
% hObject    handle to scale (see GCBO)
% eventdata  reserved - to be defined in a future version of MATLAB
% handles    structure with handles and user data (see GUIDATA)

% Hints: get(hObject,'String') returns contents of scale as text
%        str2double(get(hObject,'String')) returns contents of scale as a double

% --- Executes on button press in align.
function align_Callback(hObject, eventdata, handles)
% hObject    handle to align (see GCBO)
% eventdata  reserved - to be defined in a future version of MATLAB
% handles    structure with handles and user data (see GUIDATA)

% Hint: get(hObject,'Value') returns toggle state of align
```

APPENDIX E
MATLAB PROGRAM DEVELOPED TO AVERAGE FIELD QUADRANTS AND PRODUCE FINAL MAP OF OFF AXIS RATIOS

```
%This program is called by separate_exp when the Combine button is pressed.
% The user is prompted to select six exposures.  User needs to click on the background
% for each exposure.  Average background is subtracted from these exposures
% and exposures are stored in an array.  Program then splits each image
% matrix into four equal quadrants and stores them in a separate array.

%num=get(handles.numexp,'Value');    %returns selected item from numexp

%Enter scale  and number of exposures here (mm/pixel)
scale=0.1;
numexp=2;

%ENTER FIT PARAMETERS TO CONVERT OD TO DOSE
a=-14.82;
b=224.21;
c=2.861;
for t=1:numexp

   [scanfile,direc]=uigetfile('*.tif','Select image' );
   cd(direc);
   fid1=fopen(scanfile);
   if fid1 ~=-1
      I=imread(scanfile,'tif');

   else
      fprintf('File not found\n');
      return;
   end

   I3=double(I);
   [numpixel,B]=size(I3);

%CONVERT TO OPTICAL DENSITY
I3=-log10((I3+1)/256);
I2(t,:,:)=I3;
A=B;

          N=zeros(500,1);
          [N1,X]=hist(I3,500);

          % Combine all row histograms into a single histogram (X contains bin centers)

                  for i=1:A
                    N(:,1)=N(:,1) + N1(:,i);
    end
```

```
bar(X,N); grid on; Xlabel('Optical Density'); Ylabel('Frequency');
pbaspect([1 1 1]);Title('Histogram');

%Select background
[bkg(t),y]=ginput(1);

end

%Determine and subtract average background
avebkg=sum(bkg(:))/numexp;

I2(:,:,:)=I2(:,:,:)-avebkg;

pix=numpixel/2;

%Convert optical density to dose
for t=1:numexp
   for i=1:numpixel
      for j=1:B
         I2(t,i,j) = a*(I2(t,i,j))^2 + b*I2(t,i,j) + c;
         if I2(t,i,j)<0
            %I2(t,i,j)=0;
         end
      end
   end
end

%Declare array for the sections

Combine=zeros((numexp*4),pix,pix);
q=1;
%Split up the four images into four quadrants and store in array
for m=1:numexp

P=zeros(pix,pix);
Q=zeros(pix,pix);
R=zeros(pix,pix);
S=zeros(pix,pix);

%Upper left hand corner
for i=1:pix
   for j=1:pix
      P(i,j)=I2(m,i,j);
   end
end
P=fliplr(P);
Combine(q,:,:)=P;
q=q+1;
%Upper right hand corner
for i=1:pix
   for j=(pix+1):(numpixel)
      k=j-(pix);
      Q(i,k)=I2(m,i,j);
   end
end
Combine(q,:,:)=Q;
```

```
q=q+1;
%Lower left hand corner
for i=(pix+1):(numpixel)
   for j=1:pix
      k=i-(pix);
      R(k,j)=I2(m,i,j);
   end
end
R=fliplr(R);
R=flipud(R);
Combine(q,:,:)=R;
q=q+1;
%Lower right hand corner
for i=(pix+1):(numpixel)
   for j=(pix+1):(numpixel)
      k=i-(pix);
      l=j-(pix);
      S(k,l)=I2(m,i,j);
   end
end
S=flipud(S);
Combine(q,:,:)=S;
q=q+1;

end

%Determine the average
sum=zeros(pix,pix);
Temp=zeros(pix,pix);
for i=1:(4*numexp)
   for j=1:pix
      for k=1:pix
         Temp(j,k)=Combine(i,j,k);
      end
   end
   sum=sum+Temp;
end

Average=zeros(pix,pix);
Average=sum(:,:)/(numexp*4);
UncAverage = Average;
max(max(Average));

Average=flipud(Average);

%SUBTRACT THE AVERAGE MINIMUM
[A,B]=size(Average);
k=1;
for i=A-25:A
   l=1;
   for j=B-25:B
      sample(k,l)=Average(i,j);
      l=l+1;
   end
   k=k+1;
end
```

```
minim=mean(mean(sample));
Average = Average(:,:) - minim;

%Normalize the data to the maximum value
maxim=max(max(Average));
Average=Average(:,:)/maxim;
temp=Average;

sumdev=zeros(pix,pix);
%DETERMINE THE STATISTICAL ERROR OF THE AVERAGE
Temp2=zeros(pix,pix);
for i=1:(numexp*4)
   for j=1:pix
      for k=1:pix
         Temp(j,k)=Combine(i,j,k);
      end
   end

   for j=1:pix
      for k=1:pix
         Temp2(j,k)=(Temp(j,k)-UncAverage(j,k))^2;
      end
   end
   sumdev=sumdev+Temp2;
end

Unc=zeros(pix,pix);
Unc=sqrt(sumdev(:,:)/(numexp*4-1));
Unc=Unc./maxim;

%PLOT HISTOGRAM OF UNCERTAINTY
          N=zeros(500,1);
          [N1,X]=hist(Unc,500);

          % Combine all row histograms into a single histogram (X contains bin centers)

                    for i=1:275
                      N(:,1)=N(:,1) + N1(:,i);
    end
    N=N(:,1)/75625;

bar(X,N); grid on; Xlabel('Relative Uncertainty'); Ylabel('Relative Frequency');
pbaspect([1 1 1]);Title('Histogram'); xlim([0 .15]);

Xax=(0:274)./10;
Xtr=(274:-1:0)./10;
figure
imagesc(Xax,Xtr,Unc);colorbar;
Xlabel('Crossplane Distance (mm)');
 Ylabel('Inplane Distance (mm)');
 set(gca,'Ydir','normal');

figure
 [C,h] = contour(Xax,Xax,Average,[.9 .5 .1]); clabel(C,h);
 Xlabel('Crossplane Distance (mm)');
 Ylabel('Inplane Distance (mm)');
```

```
 legend(h,'90% isodose line','50% isodose line','10% isodose line');figure


% flip=flipud(temp);
% C=cat(1,temp,flip);
%
% flip=fliplr(temp);
% flip2=flipud(flip);
% D=cat(1,flip,flip2);
%
% final=cat(2,D,C);
%
%
% imagesc(final);
% colorbar
figure
line=Average(1,:);
plot(line,':b');
```

LIST OF REFERENCES

1. F. M. Khan, "Stereotactic Radiosurgery," in *The Physics of Radiation Therapy,* edited by J. Pine, M. Standen, L. R. Kairis, and T. Boyce (Williams & Wilkins, Baltimore, 2003).

2. F. J. Bova, W. A. Friedman, J. M. Buatti, and W. M. Mendenhall, *Linac Radiosurgery: A Practical Guide*, (Springer, New York, 1998).

3. E. J. Hall, *Radiobiology for the Radiobiologist,* (Williams & Wilkins, Baltimore, 2000).

4. R. M. Cardinal, S. H. Benedict, Q. Wu, R. D. Zwicker, H. E. Gaballa, and R. Mohan, "A comparison of three stereotactic radiotherapy techniques; arcs vs. noncoplanar fixed fields vs. intensity modulation," Int. J. Radiat. Oncol., Biol., Phys. **42**, 431-436 (1998).

5. T. H. Wagner, *Optimal Delivery Techniques for Intracranial Stereotactic Radiosurgery Using Circular and Multileaf Collimators*: PhD dissertation, Nuclear Engineering Sciences, University of Florida, Gainesville, FL (2000).

6. T. D. Solberg, K. L. Boedeker, R. Fogg, M. T. Selch, and A. A. F. DeSalles, "Dynamic arc radiosurgery field shaping: a comparison with static field conformal and noncoplanar circular arcs," Int. J. Radiat. Oncol., Biol., Phys. **49**, 1481-1491 (2001).

7. T. J. St. John, *Intensity-Modulated Radiosurgery Treatment Planning By Fluence Mapping Optimized Multi-isocenter Plans*: PhD dissertation, Nuclear Engineering Sciences, University of Florida, Gainesville, FL (2002).

8. P. G. Archer, J. M. Balter, D. A. Ross, J. A. Hayman, and H. M. Sandler, "The treatment planning of segmental, conformal stereotactic radiosurgery utilizing a standard multileaf collimator," Med. Dosim. **24**, 13-19 (1999).

9. J. L. Nakamura, A.Pirzkall, M. P. Caro., P. Xia, V. Smith, w. M. Wara, P. L. Petti, L. J. Verhey, and P. K. Sneed, "Comparison of intensity-modulated radiosurgery with gamma knife radiosurgery for challenging skull base lesions," Int. J. Radiat. Oncol., Biol., Phys. **55**, 99-109 (2003).

10. S. H. Benedict, R. M. Cardinale, Q. Wu, R. D. Zwicker, W. C. Broaddus, and R. Mohan, "Intensity-modulated stereotactic radiosurgery using dynamic micro-multileaf collimation," Int. J. Radiat. Oncol., Biol., Phys. **50**, 751-758 (2001).

11. A. S. Shiu, H. M. Kooy, J. R. Ewton, S. S. Tung, J. Wong, K. Antes, and M. H. Maor, "Comparison of miniature multileaf collimation (mMLC) with circular collimation for stereotactic treatment," Int. J. Radiat. Oncol., Biol., Phys. **37**, 679-688 (1997).

12. J. Sun and Y. Zhu, "Study of dosimetric penumbra due to multileaf collimation on a medical linear accelerator," Int. J. Radiat. Oncol., Biol., Phys. **32**, 1409-1417 (1995).

13. K. R. Rice, J. L. Hansen, and G. K. Svensson, "Measurement of dose distribution in small beams of 6MV x-rays," Phys. Med. Biol. **32**, 1087-1099 (1987).

14. D. M. Duggan and C. W. Coffey II, "Small photon field dosimetry for stereotactic radiosurgery," Med. Dosim. **23,** 153-159 (1998).

15. J. L. Robar and B. G. Clark, "The use of radiographic film for linear accelerator stereotactic radiosurgical dosimetry," Med. Phys. **26**, 2144-2150 (1999).

16. J. W. Sohn, J. F. Dempsey, T. S. Suh, and D. A. Low, "Analysis of various beamlet sizes for IMRT with 6 MV photons," Med. Phys. **30**, 2432-2439 (2003).

17. S. L. Meeks, F. J. Bova, S. Kim, W. A. Tome, and J. Buatti, "Dosimetric characterization of a double-focused miniature multileaf collimator," Med. Phys. **26**, 729-733 (1999).

18. H. E. Johns and J. R. Cunningham, *The Physics of Radiology*. New York: John Wiley & Sons (1983).

19. T. Kron, A. Elliot, and P. Metcalfe, "The penumbra of 6 MV x-ray beams as measured by thermoluminescent dosimetry and evaluated using an inverse square root function," Med. Phys. **20**, 1429-1438 (1993).

20. M. Sastre-Padro, U. A. van der Heide, and H. Welleweerd, "An accurate calibration method of the multileaf collimator valid for conformal and intensity modulated radiation treatments," Phys. Med. Biol. **49**, 2631-2643 (2004).

BIOGRAPHICAL SKETCH

Brandon K. Rice was born in October 1981, in Duluth, MN. He attended the University of Wisconsin-River Falls from 1999-2003, earning a Bachelor of Science degree in physics (with honors) in May 2003. During his undergraduate work, he served as a research assistant in the Department of Physics; he served as president of Phi Sigma Kappa national fraternity; he was a member of Sigma Pi Sigma physics honor society, and Phi Kappa Phi national honor society; and was an active member in the local chapter of the Society of Physics Students.

He entered graduate school at the University of Florida in August 2003. There he completed a Master of Science degree in medical physics. During his work, he served as a graduate research assistant in the Radiosurgery and Radiobiology Laboratory at the University of Florida Brain Institute and served as vice president of the Society of Health and Medical Physics Students. He is also a member of the American Association of Physicists in Medicine and the American Nuclear Society.